INFORMATION TO USERS

This manuscript has been reproduced from the microfilm master. UMI films the text directly from the original or copy submitted. Thus, some thesis and dissertation copies are in typewriter face, while others may be from any type of computer printer.

The quality of this reproduction is dependent upon the quality of the copy submitted. Broken or indistinct print, colored or poor quality illustrations and photographs, print bleedthrough, substandard margins, and improper alignment can adversely affect reproduction.

In the unlikely event that the author did not send UMI a complete manuscript and there are missing pages, these will be noted. Also, if unauthorized copyright material had to be removed, a note will indicate the deletion.

Oversize materials (e.g., maps, drawings, charts) are reproduced by sectioning the original, beginning at the upper left-hand corner and continuing from left to right in equal sections with small overlaps. Each original is also photographed in one exposure and is included in reduced form at the back of the book.

Photographs included in the original manuscript have been reproduced xerographically in this copy. Higher quality 6" x 9" black and white photographic prints are available for any photographs or illustrations appearing in this copy for an additional charge. Contact UMI directly to order.

U·M·I

University Microfilms International
A Bell & Howell Information Company
300 North Zeeb Road, Ann Arbor, MI 48106-1346 USA
313 761-4700 800 521-0600

Order Number 9304656

Propagation modeling and measurements of a direct sequence spread spectrum signal at 1.956 GHz for mobile communications

Erceg, Vinko, Ph.D.

City University of New York, 1992

U·M·I
300 N. Zeeb Rd.
Ann Arbor, MI 48106

PROPAGATION MODELING AND MEASUREMENTS OF A DIRECT SEQUENCE SPREAD SPECTRUM SIGNAL AT 1.956 GHz FOR MOBILE COMMUNICATIONS

by

Vinko Erceg

A dissertation submitted to the Graduate Faculty in Engineering in partial fulfillment of the requirements for the degree of Doctor of Philosophy, The City University of New York.

1992

This manuscript has been read and accepted for the Graduate Faculty in Engineering in satisfaction of the dissertation requirement for the degree of Doctor of Philosophy.

September 12, 1992
Date

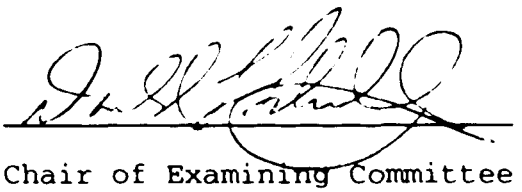

Chair of Examining Committee

September 16, 1992
Date

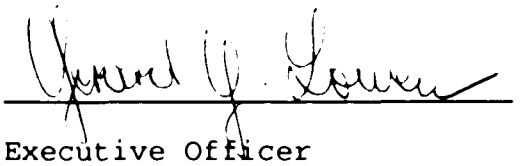

Executive Officer

Professors:

Tarek Saadawi

Svetislav Maric

Joseph Barba

Dhadesugoor Vaman

Supervisory committee

THE CITY UNIVERSITY OF NEW YORK

ABSTRACT

PROPAGATION MODELING AND MEASUREMENTS OF A DIRECT SEQUENCE SPREAD SPECTRUM SIGNAL AT 1.956 GHz FOR MOBILE COMMUNICATIONS

by

Vinko Erceg

Adviser: Professor Donald L. Schilling

The demand for increasing capacity in personal communication systems requires the use of smaller cells (microcells). The emitted power when using microcells will be of the order of milliwatts and the size of the microcells will be about 200 m. Therefore, accurate signal strength predictions become crucial when hand-off, power control, and cell planning are considered to minimize intercell interference. An accurate service-area prediction is necessary to design urban area base station layouts for microcells, and such design should be based on an understanding of the radio propagation characteristics. In this thesis the line-of-sight (LOS) and the out-of-sight propagation models based on theory and experiments were proposed. The measurements were performed for the line-of-sight and out-of-sight conditions in rural, suburban, and urban environments. In the LOS case, propagation path loss can be characterized by two slopes and a single breakpoint. The path loss along the out-of-sight streets was found to have two

distinct characteristics: The first is a sudden power level drop (corner attenuation) and the second is a difference slope (attenuation vs. distance) which follows the sudden corner attenuation.

PREFACE

This thesis is a study of the signal propagation in the microcellular environment. Accurate propagation modeling is vital for predicting the coverage and capacity of cellular systems. Rapid growth in the demand for mobile communications has created an interest in small-cell, high-capacity, mobile radio systems. A microcellular approach consists of using small cell sites which have radii in the order of 200m-1km. Only recently there have been attempts to characterize signal propagation within these short distances. Current cellular systems have cell sizes which have much larger radii. The objective in this thesis is to present accurate signal propagation models for different environments. Measurement procedures are described in Section 4. Line-of-sight propagation is presented in Section 5 and out-of-sight propagation is presented in Section 6.

ACKNOWLEDGEMENTS

I would like to express my sincere thanks and gratitude to my mentor, Professor Donald L. Schilling, for excellent guidance throughout the course of this research.

Special thanks to my dear parents and sister for their endless support. Without their support and my sisters cooking, my education would never be completed.

Particular thanks to engineers at SCS Mobilecom Inc. for their assistance in designing the measuring equipment, and to my colleagues at City College, Saeed Ghassezadeh, Maxwell Taylor and Dong Li for their help in conducting the experiments.

TABLE OF CONTENTS

LIST OF FIGURES

1 INTRODUCTION

Increasing the capacity and quality of the next generation of cellular systems has become very important in telecommunications. It has been suggested that microcellular, high-capacity, personal communication networks (PCN) be established in the 2 GHz-band using Broadband Code Division Multiple Access (B-CDMA) spread spectrum communication systems. The use of smaller cells [1-4], perhaps of 200m radius would increase the number of users and also improve communication. The use of smaller cells in urban areas would result in line of sight between user and cell most of the time. Another method to improve the quality of personal communication system is to use (B-CDMA) spread spectrum system [5-8]. Direct Sequence (DS) spread spectrum achieves a spreading of the spectrum by modulating the original signal with a very wideband signal relative to the data bandwidth. The modulation technique is binary phase shift keying (BPSK). Thus, if the original signal is s(t), where

$$s(t) = \sqrt{2P_s}\, d(t) \cos(\omega_o t)$$

the DS spread spectrum signal is

$$v(t) = g(t)\, s(t) = \sqrt{2P_s}\, g(t)\, d(t) \cos(\omega_o t)$$

where g(t) is a pseudo-random noise (PN) binary sequence having the values +1 or -1. Multiplying the BPSK sequence s(t) by g(t) spreads the spectrum. In CDMA, each user is assigned a different PN code. These codes are almost uncorrelated with one another. The number of simultaneous users depends on the cross-correlation properties of the spreading codes. For example, if user 1 has a sequence S1, and user 2 has a sequence S2 etc., then a receiver, to listen to user 1 will receive at its antenna all of the energy sent by all of the users. However, if the cross-correlation of the codes is small, the receiver will see all the energy of user 1, but only a fraction of the other users. CDMA also offers features such as multipath immunity, virtually unlimited addressing, privacy, better throughput, error correcting coding etc. Multipath is often a fundamental limitation to system performance, and spread spectrum is well known technique to combat multipath. Multipath propagation is a phenomenon when the transmitted signal takes multipath paths to the receiver and each path arrives delayed from the others and with the different power. The amount of the signal's received power can vary dramatically if the transmitter is in motion. The amount of this power variation, called fading, can be more than 40 dB for narrowband signals [9,10]. The reason for this is that when the narrowband signal propagates, its coherence bandwidth (the range of frequencies which fade together) is larger than the signal bandwidth. Since the observed fading due to multipath is usually not significantly wider than 15 MHz, the power loss due to the fading of the B-CDMA system whose

bandwidth is wider than 15 MHz is less [6,7,11,12]. This is a big advantage of the B-CDMA system over other systems used in the mobile communications.

2 REVIEW OF THE PRIOR WORK

Other investigators have attempted to obtain a model for the propagation loss [13-27]. However, they were limited in the amount of data taken and also by their use of a relatively narrowband transmitted waveform. Thus, the results were, for the most part, as pointed by Green and Hata [25], not repetitive. The results obtained here are extensive with data taken each centimeter. B-CDMA was used for transmission and therefore the results were found to be repetitive. In the past, the propagation model of Hata [23] has often been used. These are the empirical formulae and do not give accurate propagation attenuations at the short distances. Rustako et al. [24] used a two-ray and a six-ray model to calculate the received power in rural and urban environments, respectively. It was found that the propagation attenuation followed two laws: One is an inverse square-law dependence at the closer range and an inverse fourth-law dependence at the further range when there exists LOS between the transmitting antenna and the receiving antenna. Harley [26] also investigated the short range propagation attenuation and proposed a model with two slopes and a breakpoint. At the breakpoint, the propagation attenuation assumed a steeper slope than one before the breakpoint. Most recently, Green and Hata [25] used experimental data to approximate the path loss by a free space characteristic close to the base site before changing to the faster attenuation rate of an inverse fourth power law. Their analysis of the results suggested a large spread in the

reported breakpoint value which tended toward a mean given by

$$d_o = \frac{2\pi h_1 h_2}{\lambda}$$

All of the above authors described, empirically, the distance at which the breakpoint occurs. Out-of-sight propagation experiments and modeling for the perpendicular location of the streets [29] were performed using a narrowband signal in the Tokyo metropolitan area. Based on the experimental data, the following results were obtained; (a) the wider the out-of-sight roads, the stronger the received power, (b) if the distance d_1 from the base station to a corner to be turned becomes greater, the received signal suffers from the greater attenuation, (c) when the distance d_1 becomes greater, the attenuation vs. distance slope after the turning becomes greater.

3 CONTRIBUTION

In this thesis a model which gives the upper and lower bounds on the power of the received DS spread spectrum signal is presented. The approximate breakpoint in the bound which separates two slopes is described mathematically from the classical two-ray model. The extensive propagation measurements were taken at different locations and it was found that the location of the breakpoint as well as its power level are not considerably effected by different environments when LOS exists. Signal power levels for the out-of-sight conditions were also investigated in the suburban and urban areas. A model is proposed for the perpendicular position of the streets, which is very common environmental planning in any urban and suburban area around the world.

Experiments were performed in Long Island, New York City, San Diego, and Houston. Most measurements were up to 2 km; however, some of Houston measurements were up to 8 km.

4 MEASUREMENT SET-UP

The experimental equipment consisted of a log amplifier, a wheel with photo interrupter, and a computer with an analog to digital converter board. A schematic of the measuring equipment is shown in Fig.4.1. The RF input was connected to the log amplifier and the amplifier's output voltage level was connected to the analog to digital converter board. The photo-interrupter was installed on the wheel which was marked with white dots. Each time a dot would pass in front of the photo-interrupter, the analog to digital converter board was activated and data was captured by the computer. The response time of the system was 0.5 ms and its measuring range was 7 decades, from -25 dBm to -95 dBm. The system was calibrated in the laboratory using a HP power meter and a B-CDMA spread spectrum signal. The equipment was placed in a mobile vehicle with the wheel affixed to the side of the vehicle. The average speed of the vehicle while taking measurements was 35 km/h. The spread spectrum transmitter employed DS spread spectrum with a 48 MHz bandwidth. The maximum transmitted power was 37 dBm. Two omnidirectional antennas with ground plane and a 5.6 dB gain at an elevation angle of 25 degrees were used. Antenna heights were varied from 1.5 m to 13.1 m.

5 LOS PROPAGATION

5.1 Two-Ray Model [27,28,30]

Figure 5.1.1 shows two antennas, one at a height h_1 and the other at a height h_2. When transmitting between these antennas there are two received rays, a direct ray and a ground reflected ray. The free-space field intensity of the direct ray is given by

$$E_o = \frac{\sqrt{30\ g_1\ P_t}}{d_1} \qquad (5.1.1)$$

where d_1 is the path length of the direct ray, g_1 is the gain of the antenna and P_t is the power transmitted. The electric field E_r at point b is the sum of the reflected and direct ray. Thus,

$$E_r = E_o\left(1 + \frac{d_1}{d_2 + d_3} R(\phi)\, e^{j\Delta}\right) \qquad (5.1.2)$$

where $R(\phi)$ is the reflection coefficient, ϕ is the angle between ground and the reflected ray, and Δ is the phase difference between two rays. It is readily shown, from Fig.5.1.1 that

$$\Delta = \frac{2\pi}{\lambda}\left[(d_2+d_3)-d_1\right] = \frac{2\pi}{\lambda}\left[\left\{d^2+(h_1+h_2)^2\right\}^{1/2}-\left\{d^2+(h_1-h_2)^2\right\}^{1/2}\right]$$
$$\approx \frac{2\pi}{\lambda}\left\{d\left[1+\frac{(h_1+h_2)^2}{2d^2}\right]-d\left[1+\frac{(h_1-h_2)^2}{2d^2}\right]\right\} \qquad (5.1.3)$$
$$\approx \frac{4\pi h_1 h_2}{\lambda d}$$

The received power is then

$$P_r = \left(\frac{E_t\lambda}{2\pi\sqrt{120}}\right)^2 g_2 \qquad (5.1.4)$$

Hence,

$$P_r = \left(\frac{\lambda}{4\pi}\right)^2\left\{\frac{\sqrt{g_1(\alpha_1)\,g_2(\beta_1)\,P_t}}{d_1}+R(\phi)\,\frac{\sqrt{g_1(\alpha_2)\,g_2(\beta_2)\,P_t}}{d_2+d_3}\,e^{j\Delta}\right\}^2 \qquad (5.1.5)$$

Letting

$$A = \frac{\sqrt{g_1(\alpha_1)\,g_2(\beta_1)\,P_t}}{d_1}$$

and

$$B = R(\phi)\,\frac{\sqrt{g_1(\alpha_2)\,g_2(\beta_2)\,P_t}}{d_2+d_3}$$

we have

$$P_r=\left(\frac{\lambda}{4\pi}\right)^2 (A+Be^{j\Delta})\,(A+Be^{-j\Delta})$$
$$=\left(\frac{\lambda}{4\pi}\right)^2 (A^2+B^2+2AB\cos\Delta) \qquad (5.1.6)$$

If we assume vertical polarization, the reflection coefficient is

$$R(\phi)=\frac{\epsilon_o\sin\phi-\sqrt{\epsilon_o-\cos^2\phi}}{\epsilon_o\sin\phi+\sqrt{\epsilon_o-\cos^2\phi}} \qquad (5.1.7)$$

and

$$\epsilon_o=\epsilon-j60\sigma\lambda$$

where the dielectric constant ϵ is typically ϵ = 15 for a road or other hard surface and σ is the conductivity of the ground in mhos per meter. The angle ϕ is shown in Fig.5.1.1. A computer evaluation was performed of the received power P_r as a function of distance. The result is shown in Fig.5.1.2. We can see that the resulting curve can be upper bounded by a 2-slope piecewise linear curve. The first slope is approximately 1.7 and the second slope is 4.0. The approximate breakpoint distance can be calculated using an approximation for d, R and g at far distances. Assume unity gain of the antennas and R = -1. Then using Eq.5.1.6

$$P_r=\left(\frac{\lambda}{2\pi d}\right)^2 \sin^2\frac{\Delta}{2}\,P_t \qquad (5.1.8)$$

To calculate the breakpoint, set

$$\frac{\Delta}{2} = \frac{\pi}{2}$$

Hence,

$$\frac{2\pi h_1 h_2}{\lambda d} = \frac{\pi}{2}$$

and the approximate distance of the breakpoint is

$$d_o \approx \frac{4 h_1 h_2}{\lambda} \qquad (5.1.9)$$

After the breakpoint sin $\Delta/2$ can be approximated by $\Delta/2$. Equation 5.1.8 then becomes (using Eq.5.1.3)

$$P_r = \left(\frac{\lambda \Delta}{4\pi d}\right)^2 P_t = \frac{(h_1 h_2)^2}{d^4} P_t \qquad (5.1.10)$$

Note that P_r decreases as an inverse fourth power beyond the breakpoint and not as an inverse square law (free space propagation). The approximate distances of all other maxima occur when $(h_1+h_2) \ll d \leq d_o$ and can be calculated from Eq.5.1.3 by setting $\Delta = \pi(2n+1)$. Then,

$$d_n\left[1+\frac{(h_1+h_2)^2}{2d_n^2}\right]-d_n\left[1+\frac{(h_1-h_2)^2}{2d_n^2}\right]=(2n+1)\lambda \qquad (5.1.11)$$

After simplifying, the maxima occur at

$$d_n \approx \frac{4h_1h_2}{(2n+1)\lambda} \qquad for \quad n=0,1,2... \qquad (5.1.12)$$

When n=0, the distance d_o becomes the location where the last maximum occurs which verifies Eq.5.1.9. Equation 5.1.6 is dependent on the frequency, the antenna heights, and the reflection coefficient. If the transmitting antenna height is increased, the breakpoint shifts further away. If the reflection coefficient approaches zero, the slope approaches 2.0 which is the free space propagation law. To calculate the approximate distances at which the minima occur, set

$$\Delta = 2n\pi$$

then,

$$d_n \approx \frac{2h_1h_2}{n\lambda} \qquad for \quad n=0,1,2,... \qquad (5.1.13)$$

To calculate the power at the breakpoint P_b, we set

$$\sin^2\Delta = 1$$

Hence,

$$P_b=\left(\frac{\lambda^2}{8\pi h_1 h_2}\right)^2 P_t \qquad (5.1.14)$$

The path loss L_b (positive quantity) at the breakpoint can be calculated using

$$L_b=\left|10\log\left[\left(\frac{\lambda^2}{8\pi h_1 h_2}\right)^2\right]\right| \qquad (5.1.15)$$

An approximate, empirically obtained, upper bound to the urban and suburban experimental data obtained is then given by

$$\begin{aligned} L_u&=L_b+20\log_{10}\left(\frac{d}{d_o}\right) \qquad for\ d\le d_o \\ L_u&=L_b+40\log_{10}\left(\frac{d}{d_o}\right) \qquad for\ d>d_o \end{aligned} \qquad (5.1.16)$$

In addition, an approximate lower bound to the urban and suburban experimental data is

$$\begin{aligned} L_L&=L_b+20+25\log_{10}\left(\frac{d}{d_o}\right) \qquad for\ d\le d_o \\ L_L&=L_b+20+40\log_{10}\left(\frac{d}{d_o}\right) \qquad for\ d>d_o \end{aligned} \qquad (5.1.17)$$

These bounds, plotted with experimental data, are presented in

Sec.5.3.

We conclude that for urban and suburban areas, Eqs. 5.1.16 and 5.1.17 represent the approximate upper and lower bounds to the experimental data, while for the rural area the upper bound after the breakpoint is very close to the average signal path loss. The reason for this is that the rural area propagation closely follows the two-ray propagation model of Fig.5.1.2.

5.2 N-Multipath Propagation

If we have (N+1) different paths, the received electric field is

$$E_r=\left(E_o+E_1R_1e^{j\Delta_1}+E_2R_2e^{j\Delta_2}+\ldots.+E_NR_Ne^{j\Delta_2}\right) \qquad (5.2.1)$$

Hence,

$$P_r=\sum_{i=0}^{N}\left(\frac{\lambda}{4\pi}\right)^2\left(\frac{R_i}{d_i}\right)^2P_t+\frac{2}{d_o}\sum_{i=1}^{N}\left(\frac{\lambda}{4\pi}\right)^2\frac{R_i}{d_i}P_t\cos\Delta_i + \sum_{i=1,i\neq j}^{N}\sum_{j=1}^{N}\left(\frac{\lambda}{4\pi}\right)^2\frac{R_iR_j}{d_id_j}P_t\cos\left(\Delta_i-\Delta_j\right) \qquad (5.2.2)$$

R_i and R_j can have positive or negative values depending on how many reflections were present in a particular path. For example, if there were three reflections present in a

particular path, and assuming perfect reflection so that R=-1, then

$$R_i=(-1)^3=-1$$

An even number of reflections gives a positive total reflection.

5.3 EXPERIMENTAL RESULTS (LOS)

5.3.1 Rural Area

Experiments were performed at two locations with 6.1m, 7.6m and 13.1m antenna heights. The first location was a straight road at Jones Beach, Long Island, and a second location was a straight road outside Houston, Texas. There was moderate traffic, low trees, power lines and telephone poles along the roads. The experimental results almost perfectly agree with the two-ray propagation model. Breakpoints in all measurements fall very close to the distance described by Eq.5.1.9. Typical experimental data is shown in Figs. 5.3.1 through 5.3.3. The upper and lower bounds described by Eqs. 5.1.16 and 5.1.17 are also shown on each of these graphs.

5.3.2 Urban and Suburban Areas

Experiments in the urban and suburban areas of Flushing, New York; Manhattan, New York; Port Washington, New York; and Houston, Texas were performed. The measured breakpoints and slopes also agree with two-ray model with the difference that the increased multipath produces additional lobes, and short distance fades. A straight line drawn through the maximums produces two slopes approximately 2.0 and 4.0, but the average signal level decreases as the multipath increases.

At the Flushing, New York suburban area, experiments with tree blockage were also performed. As trees became denser, the breakpoint shifted so that d_o decreased, but the slopes through the maximums did not change. It was experienced that moderate tree blockage shifted the breakpoint by a factor of 4, while heavy tree blockage made the breakpoint almost disappear and a slope of approximately 4.0 dominated [see Fig.5.3.4 and Fig.5.3.5].

The urban area measurements were performed in Midtown Manhattan and Houston Downtown areas. The Manhattan measurements were taken along 8th. Av. and also along 18th and 22nd street. The traffic was moderate. However, the environments represent a very dense urban area with high buildings where multipath is expected to be of the highest order when compared to any other environment. The Manhattan experimental data with the upper and the lower bounds is shown

in Figs. 5.3.6 through 5.3.8. The suburban area measurements were performed in Flushing, Long Island and Houston, Texas. The experimental data obtained in Flushing with the upper and the lower bounds is shown in Figs. 5.3.9 through 5.3.11. Figures 5.3.12 through 5.3.14 show the data obtained in Houston urban and suburban area using the HP power meter.

These experiments indicate a similar propagation law in the rural, suburban and urban areas. One can conclude from these results that the direct and the ground reflected ray are two dominant rays. Reflections from walls of buildings, or wall-street reflected rays account mainly for the short distance fades.

Wall reflected rays and wall-street reflected rays are scattered by the irregularities of the building surfaces and attenuated by multiple reflections. In addition, all the building fronts are not lined up and perpendicular streets leave open spaces. This indicates that such rays have a temporary effect on the propagation law, and that superimposing these rays on the two-ray model as additional multipath provides a satisfactory explanation of the experimental data obtained in the urban and suburban areas.

6 OUT-OF-SIGHT PROPAGATION

6.1 Introduction to Out-of-Sight Communication

A Model for the calculation of the path loss characteristics of a DS-CDMA system for communication which occurs when a mobile user is "Out-of-Sight" of the base station due to building blockage is presented in the following sections. The theory was verified by experimental results taken in New York City and Long Island, using antenna heights which were less than the heights of the surrounding buildings. The path loss along the out-of-sight street was found to have two distinct characteristics: The first is a sudden power level drop (corner attenuation), and the second is a different slope (attenuation vs. distance) which follows the sudden corner attenuation. For the experiments, the base station antenna was set to be at heights of 6.6m or 3.3m while the mobile antenna was fixed at a height of 1.5m.

Out-of-sight communication is defined by Fig. 6.1.1. Here we see a transmitter, street configuration and a receiver moving out-of-sight of the transmitter. The urban area experimental data was gathered in the mid-town section of New York City, with the locations of the transmitting antenna being along Park Avenue and 6th Avenue. The buildings in these regions are located next to each other and the average height of each building is approximately 30m. Each block is approximately 75m long. The width of the main streets and side streets are

approximately 30m and 20m, respectively. The suburban area experimental data was gathered in Flushing, New York with the location of the transmitting antenna along Northern Blvd. The main difference between the two environments is the relative heights of the buildings and the congestion. The Flushing buildings are approximately 12m in height.

For all measurements, the height of the transmitting antenna remained fixed at 6.6m, except for the Park Avenue measurements where a 3.3m transmitting antenna height was also used. The base station antenna and the transmitting equipment were placed about 4m away from the buildings for the 6th Avenue and Northern Blvd. measurements, while for the Park Avenue South measurements the transmitting antenna was placed in the middle of the street.

6.2 Theoretical "Out-of-Sight" Path Loss Model

The out-of-sight propagation model in urban and suburban areas with perpendicular streets and avenues has two distinct characteristics. The first characteristic is that after turning the corner, a sudden drop in power level occurs. The second characteristic is that there is a steeper slope (path loss vs. distance) along the out-of-sight streets. Both the power level drop and the steeper slopes depend upon the widths of the streets and the distance from the transmitter to the corner where the mobile receiver moves out-of-sight (turning corner distance). As the turning corner distance increases, the power level drop and the slope also increase. The reason that this drop and different slope occur, is because of the angles at which the reflected rays enter the out-of-sight streets as well as the number of rays entering the out-of-sight streets.

Figure 6.2.1 shows how the reflected rays enter the out-of-sight-street at near and far distances. From the figure we can see that the angle δ in the side streets is larger in the case of the further out-of-sight streets. This results in more reflections along the same distance when compared to the closer out-of-sight streets. The multiple reflections are the main reason for the steeper slopes. There is a greater power loss inflicted on a ray when it bounces off the building than the loss which occurs because of the increased path length, especially for the large angles δ. Depending on the number of

reflections along the particular distance, the path loss vs. distance slope increases. More reflections produce steeper slopes.

To develop the theoretical model, it was assumed that the reflected rays are dominant over the diffraction rays. In Fig.6.2.1, at each point along the distance d_2, many rays contribute to the received power. When d_2 is smaller, rays which are reflected less frequently along the walls of distance d_1, are the dominant ones. As distance d_2 increases, these rays attenuate faster than the rays which are reflected frequently along the distance d_1. The rays which are reflected more frequently along the distance d_1 are less frequently reflected along the distance d_2, and as the distance d_2 increases these rays at some point experience less attenuation than the rays which are reflected many times along the distance d_2. The power of each ray can be calculated using the classical square law propagation formula:

$$P_r = P_0 \left(\frac{\lambda}{4\pi}\right)^2 \frac{R^2}{D^2} \qquad (6.2.1)$$

Where R is the total reflection coefficient and is equal to

$$R = R^K(\gamma)\, R^M(\delta) \qquad (6.2.2)$$

For electric field perpendicular to the incidence plane

$$R(\gamma,\delta)=\frac{\sin(\gamma,\delta)-\sqrt{\epsilon_o-\cos^2(\gamma,\delta)}}{\sin(\gamma,\delta)+\sqrt{\epsilon_o-\cos^2(\gamma,\delta)}} \qquad (6.2.3)$$

and

$$\epsilon_o=\epsilon-j60\sigma\lambda \qquad (6.2.4)$$

where

- γ is the angle between the ray and the reflecting surface in the LOS street
- δ is the angle between the ray and reflecting surface in the out-of-sight street
- M is the number of reflections in the out-of-sight street
- K is the number of reflections in the LOS street
- D is the path length
- P_t is the transmitted power
- P_r is the received power
- ϵ is the dielectric constant
- σ is the conductivity in mhos/meter

The received power of all the rays which reach the receiving antenna is calculated using

$$P_r = \sum_{i=1}^{n} \left(\frac{\lambda}{4\pi}\right)^2 \frac{R_i^2}{D_i^2} P_t + \sum_{i=1}^{n} \sum_{j=1, i \neq j}^{n} \left(\frac{\lambda}{4\pi}\right)^2 \frac{R_i R_j}{D_i D_j} P_t \cos(\Delta_i - \Delta_j) \qquad (6.2.5)$$

where n is the number of rays reaching the antenna and $(\Delta_i - \Delta_j)$ is the phase difference between two rays.

In the model for the out-of-sight transmission, for simplicity, only the rays which passed through point A in Fig.6.2.2 were summed. Figure 6.2.3 shows the angle α_{11} which represents the minimum angle for which the ray leaving the transmitting antenna enters the out-of-sight street, with only one reflection along the distance d_1. The angle α_{21} represents the maximum angle for such a ray. The angle α is the angle for which the ray passes through the point A. Assuming that they reach the receiving antenna, the path length and the angle of incidence of the rays passing through point A represent the approximate path length and angle of incidence while propagating along the out-of-sight street.

Now, let us define coefficient α_i as

$$\alpha_i = \frac{\alpha_{2i} - \alpha_{1i}}{\pi} \quad , i = 1, 2 \ldots n \qquad (6.2.6)$$

The coefficient α_i is proportional to the number of rays entering the out-of-sight street and $\alpha_i \leq 1$. The same coefficient can be calculated for each of the rays passing

through point A in Figure 6.2.2. For the LOS case $\alpha_i = 1$. The second summation term in Eq.6.2.5 represents multipath fading (for the large number of rays the phase angles are assumed to be statistically independent having a uniform probability density function in the interval [0-2π]), and hence the average path loss L_r for the out-of-sight communication model is

$$L_r = \left| 10\log_{10}\left\{ \sum_{i=1}^{n} \left(\frac{\lambda}{4\pi}\right)^2 \frac{R_i^2}{D_i^2} \alpha_i \right\} \right| \quad , \alpha_i \leq 1 \qquad (6.2.7)$$

Figures 6.2.4 through 6.2.6 show the theoretical results for different turning corner distances obtained using Eq.6.2.7 as well as experimental data. The dielectric constant ε=15 and conductivity constant σ=7.5 were used. The conductivity σ can have very large values (>>1) for building surfaces and structures [9]. The value of σ was chosen to give a close match to the path loss experimental data. Unfortunately, theoretical values of σ are not available. In the theoretical analysis it was assumed that for each out-of-sight street of interest, the power leakages through the preceding streets that are negligible. This assumption was based on the fact that coefficient α_i in the LOS street is 1, while in the out-of-sight street is much less than 1, which indicates that the power leakage through the out-of-sight streets is negligible, especially when the turning corner distances are large. Figures 6.2.7 and 6.2.8 show the corner attenuation and the

slope after turning the corner as a function of the distance between the transmitter and the corner where the mobile receiver moved out-of-sight. The theoretical result obtained when the out-of-sight street width was doubled is shown in the Fig.6.2.9. As expected, the corner attenuation and the slope decreased. The number of reflections in the wider out-of-sight street decreased when compared to the narrow out-of-sight street for the same distance. Figures 6.2.10 and 6.2.11 show how the corner attenuation and the slope (attenuation vs. distance) change when the turning corner distance and the LOS street width were kept constant at 160m and 30m, respectively, while the out-of-sight street width was varied from 10m to 50m. When the location of the transmitting antenna is changed from the middle of the street to the sidewalk, the corner attenuation and the attenuation vs. distance slope changed insignificantly because the angles for which the rays enter the side streets changed very little. By moving the transmitting antenna, the distance in the street of average width changes only about 10m, while the distance to the first turning corner remains approximately 75m (the length of the average block). However, by changing the transmitting and receiving antenna heights, LOS propagation is affected, but the corner attenuation and the attenuation vs. distance slope in the out-of-sight street remain approximately the same. Again, the reason for this is a minimal change of the angles and the path lengths of the rays which enter the side streets when the antenna heights are varied. The average path loss equation for the out-of-sight street can be calculated using

$$L_o = L_F + A + (10B)\log_{10}\left(\frac{d_2 + d_1}{d_1}\right) \qquad (6.2.8)$$

where L_F is calculated using the free space propagation formula:

$$L_F = \left|20\log_{10}\left(\frac{\lambda}{4\pi d_1}\right)\right| \qquad (6.2.9)$$

where

- L_o is the path loss in the out-of-sight street
- A is the corner attenuation and is determined by
  A = L_r (immediately after turning the corner) - L_r (just before turning the corner)
- B is the slope in the out-of-sight street and is determined by the slope of L_r
- d_1 is the distance to the corner
- d_2 is the distance along the out-of-sight street

The above equation combined with Eqs.5.1.16 and 5.1.17 fully describe the LOS and out-of-sight propagation in urban and suburban environments.

6.3 Experimental Results

Extensive propagation measurements were performed in urban and suburban areas. Each of the measurements were started from the transmitting antenna into the LOS street and then a turn was made in an out-of-sight street. The sudden power level drop at the corner and the different propagation slope occurred which agreed with the theoretical model. With an increase in the distance between the transmitter and the receiver at the turning corner, both the power level drop and the slope also increased. Figures 6.2.7. and 6.2.8 compare the power level drops (relative to the free space propagation) and the slopes as a function of distance between the transmitter and the turning corner of all the experimental data to the theoretical results. We also observe that the corner attenuation and the slope are very similar in the urban and suburban areas which indicates that the same model can be used for both environments. The reason for this is that the heights of the antennas were considerably below the relative heights of the buildings as well as the widths of the streets and the lengths of the blocks were similar. Also, while moving along the out-of-sight streets, the signal power level increased at each of the intersections because of the power coming from the other streets.

Additional experimental results, which further substantiate the typical results shown above are presented in Figs.6.2.12 through 6.2.25. Figures 6.2.12 through 6.2.16 show out-of-

sight propagation along 6th Avenue in Manhattan. Here the base station antenna is at a height of 6.6m and the mobile user antenna is at a height of 1.5m. Figures 6.2.17 through 6.2.20 show the out-of-sight path loss as a function of distance along Park Avenue in Manhattan. Here the base station antenna height was lowered to 3.3m. Figures 6.2.21 through 6.2.25 show the out-of-sight results obtained in Northern Blvd., New York. Here the base station antenna is at a height of 6.6m. Note in each case the pronounced corner attenuation when moving out-of-sight.

7 CONCLUSION

A two-ray propagation model was developed employing a direct and a reflected ray. This model was verified by extensive measurements taken in urban, suburban, and rural environments. The results obtained clearly show that the data can be upper and lower bounded by a two-segment piecewise linear curve. The approximate breakpoint in the bound separating the two slopes is described mathematically from the classical two-ray model. The experimental data showed that the location of the breakpoint as well as its power level are not significantly affected by different environments when LOS exists. The results also indicate that the multi-reflection model explains the power loss along the "out-of-sight" streets. As the turning corner distance increases, the corner attenuation and the slope increase also. Extensive propagation measurements were performed to verify the theoretical results, and it was found that the experimental results are similar in urban and suburban areas. The theoretical model also predicts how the sudden power drop and the attenuation vs. distance slope decrease as the width of the out-of-sight street increases. The corner attenuation and the slope in the out-of-sight streets are not significantly affected by the different antenna heights and locations of the transmitting antenna in the microcellular environment. The results obtained are very important when cell planning, power control and hand-off are considered. To minimize intercell interference, power levels in each microcell must be set properly using accurate

propagation models. Utilizing proper designs, the LOS communication coverage of a cell can be within the square law power propagation region, while the fourth law power region becomes interference to other cells. In this way the intercell interference can be greatly reduced.

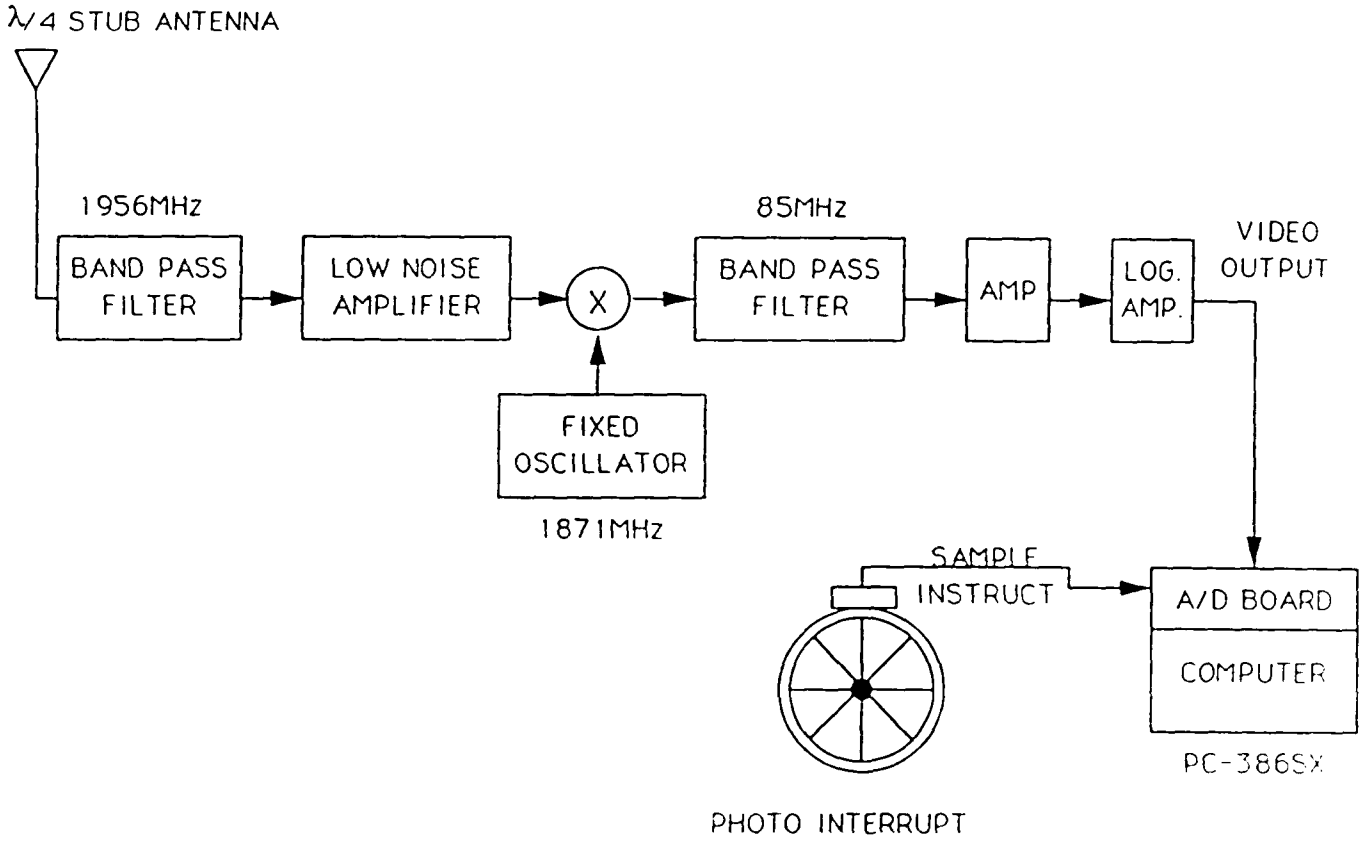

Figure 4.1 Measuring equipment

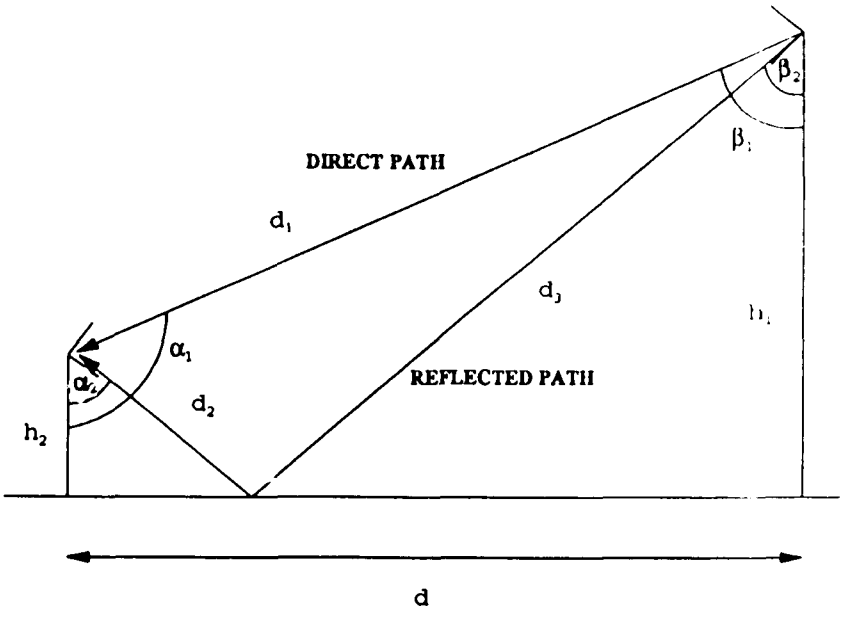

Figure 5.1.1 Two-ray propagation

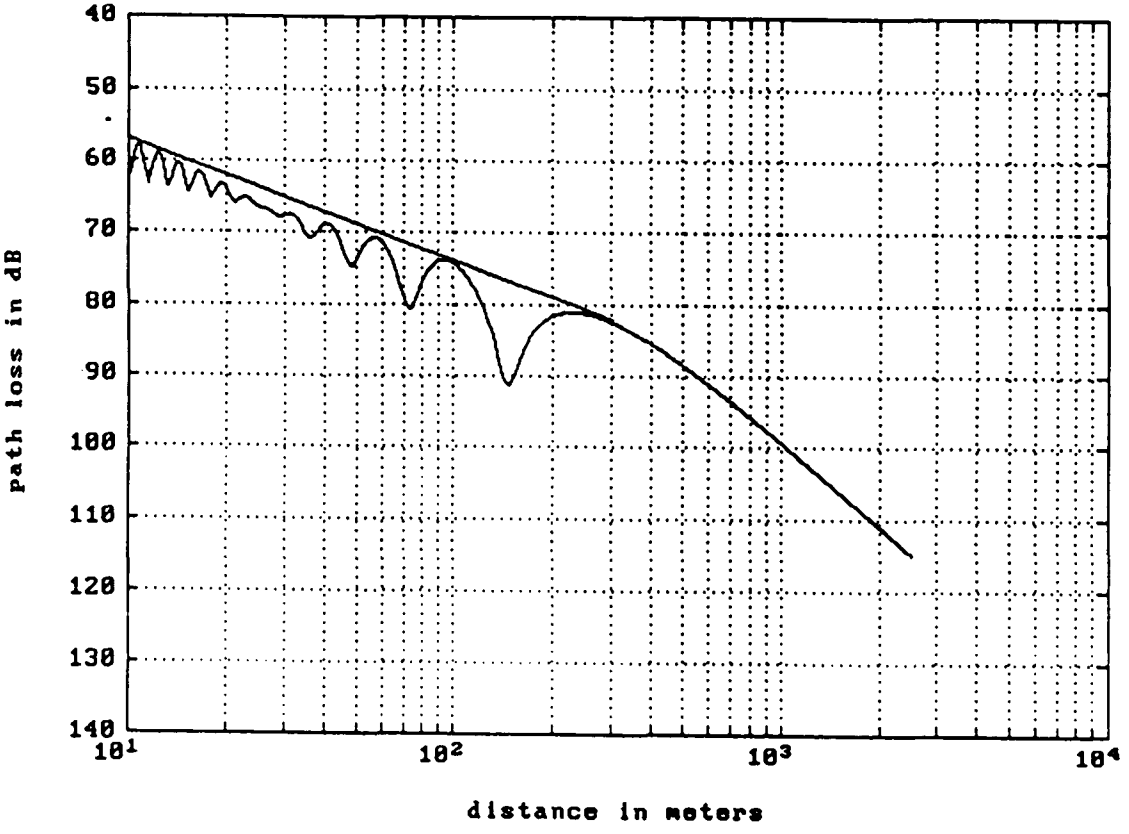

Figure 5.1.2 Two-ray propagation (computer evaluation)
h_1=7.6m, h_2=1.5m, λ=0.153m

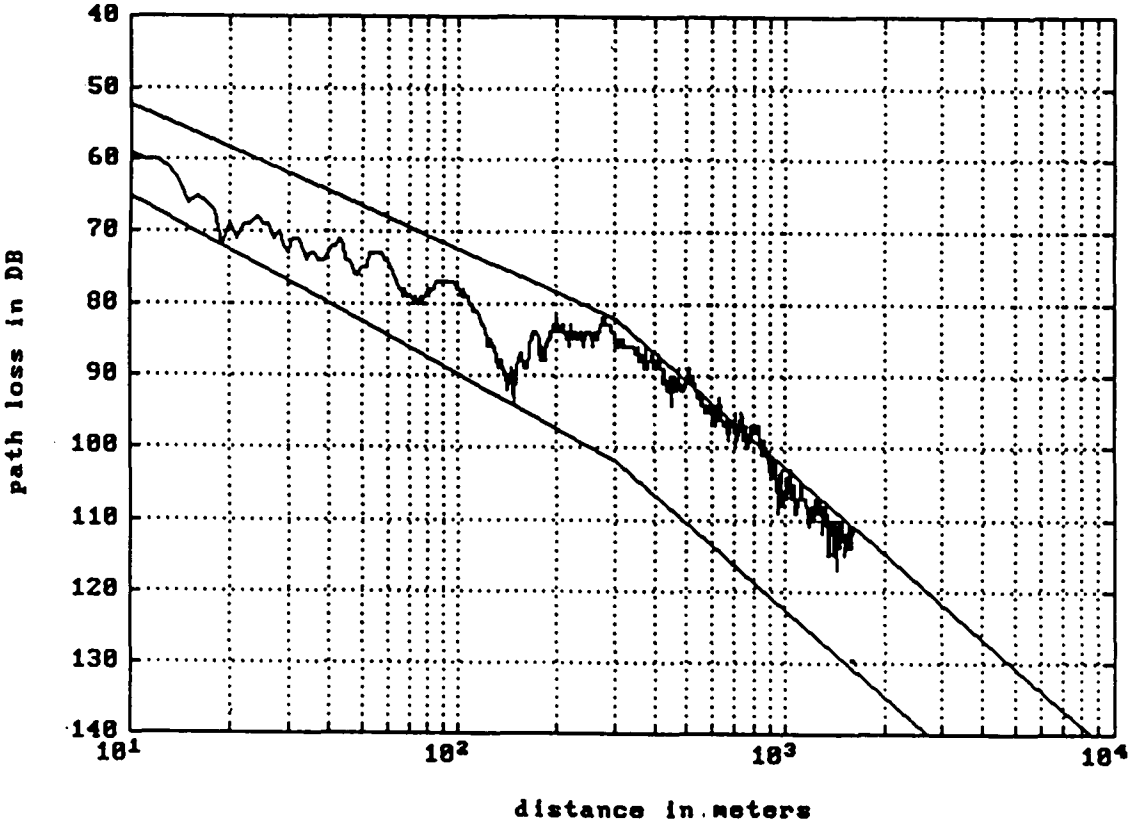

Figure 5.3.1 Rural area experimental data h_b=7.6m, h_m=1.5m

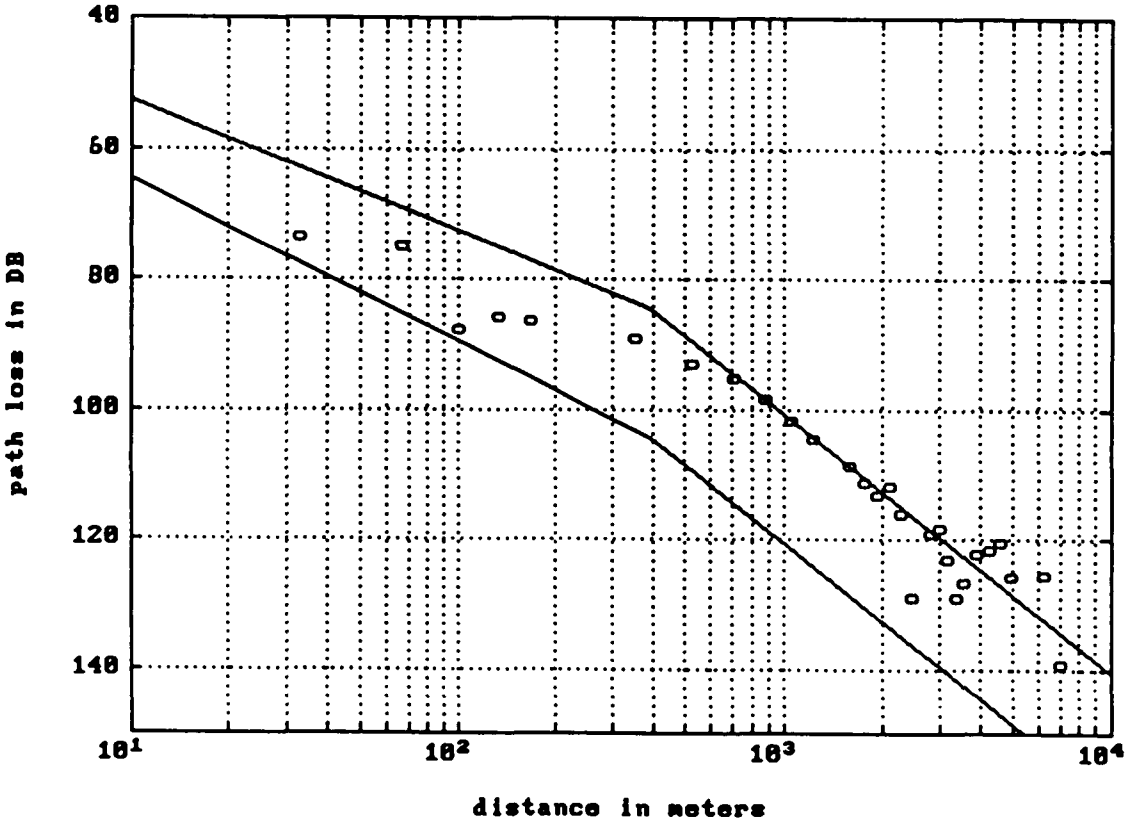

Figure 5.3.2 Rural area experimental data h_b=6.1m, h_a=2.2m

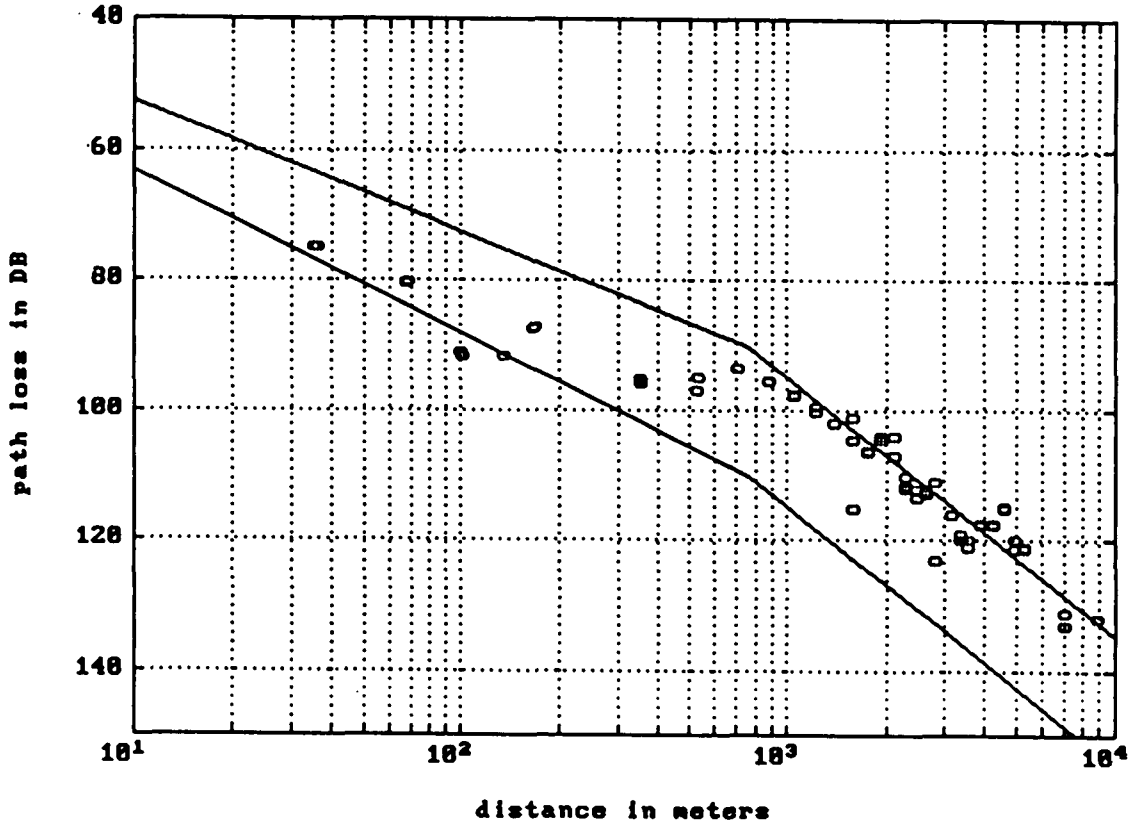

Figure 5.3.3 Rural area experimental data h_b=13.1m , h_m=2.2m

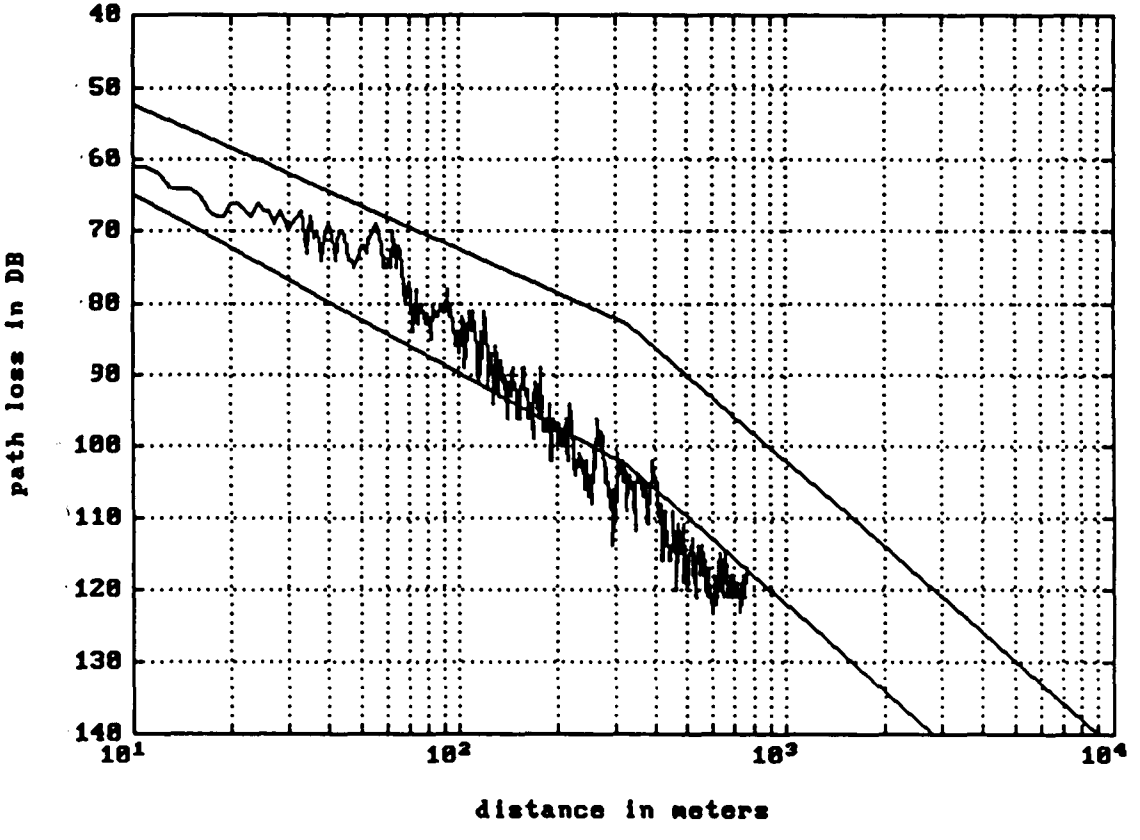

Figure 5.3.4 Suburban area experimental data with tree blockage
h_b=8.3m , h_m=1.5m

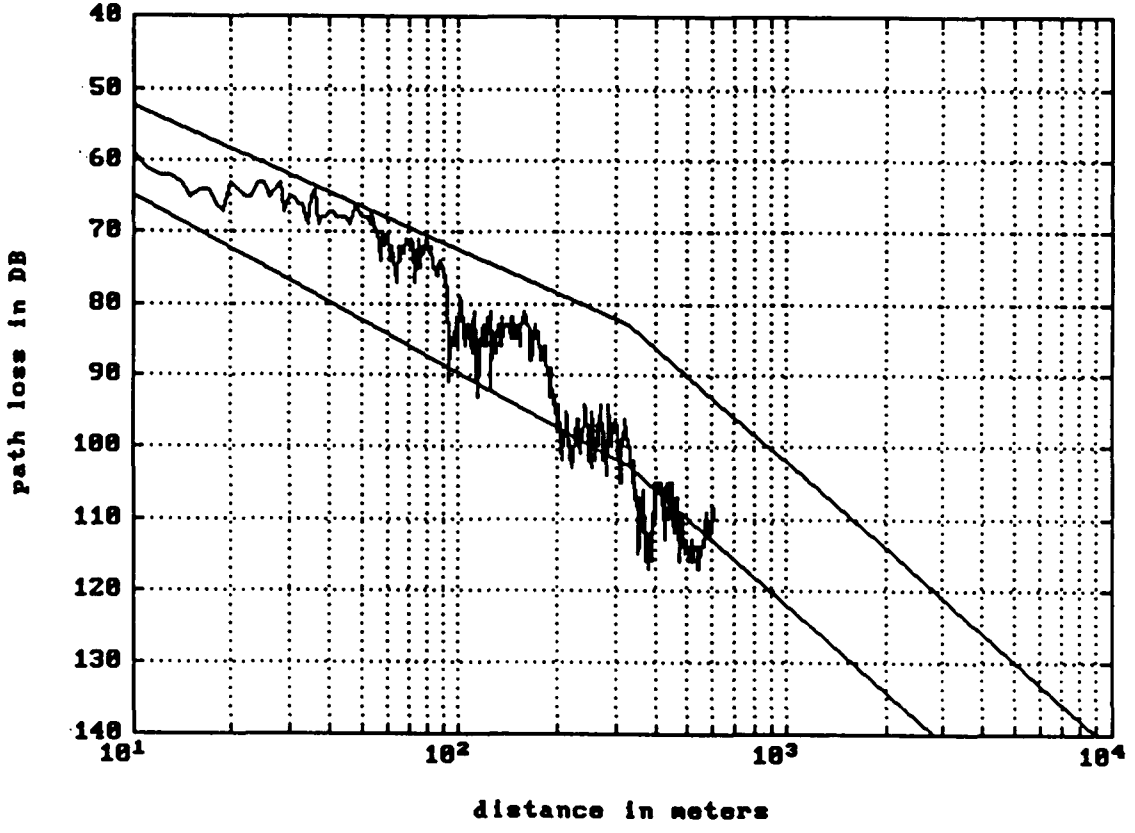

Figure 5.3.5 Suburban area experimental data with tree blockage h_b=8.3m , h_m=1.5m

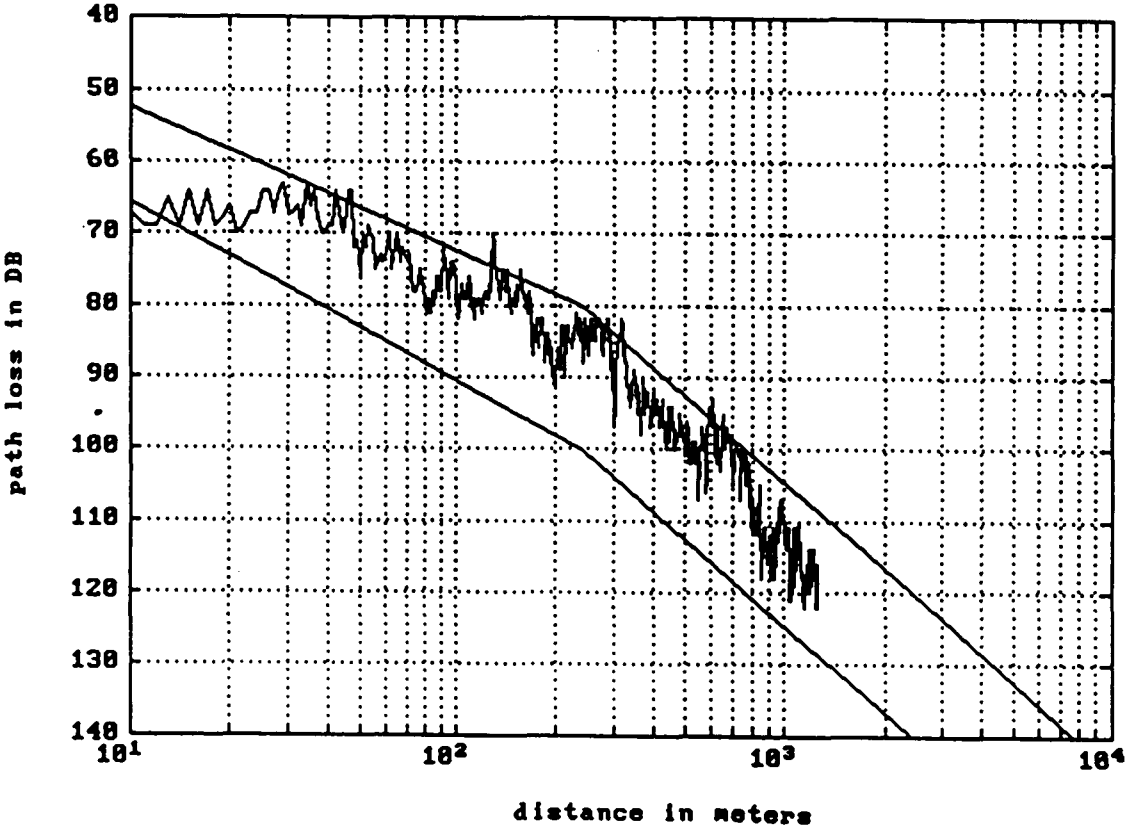

Figure 5.3.6 Urban area experimental data h_b=6.1m , h_m=1.5m

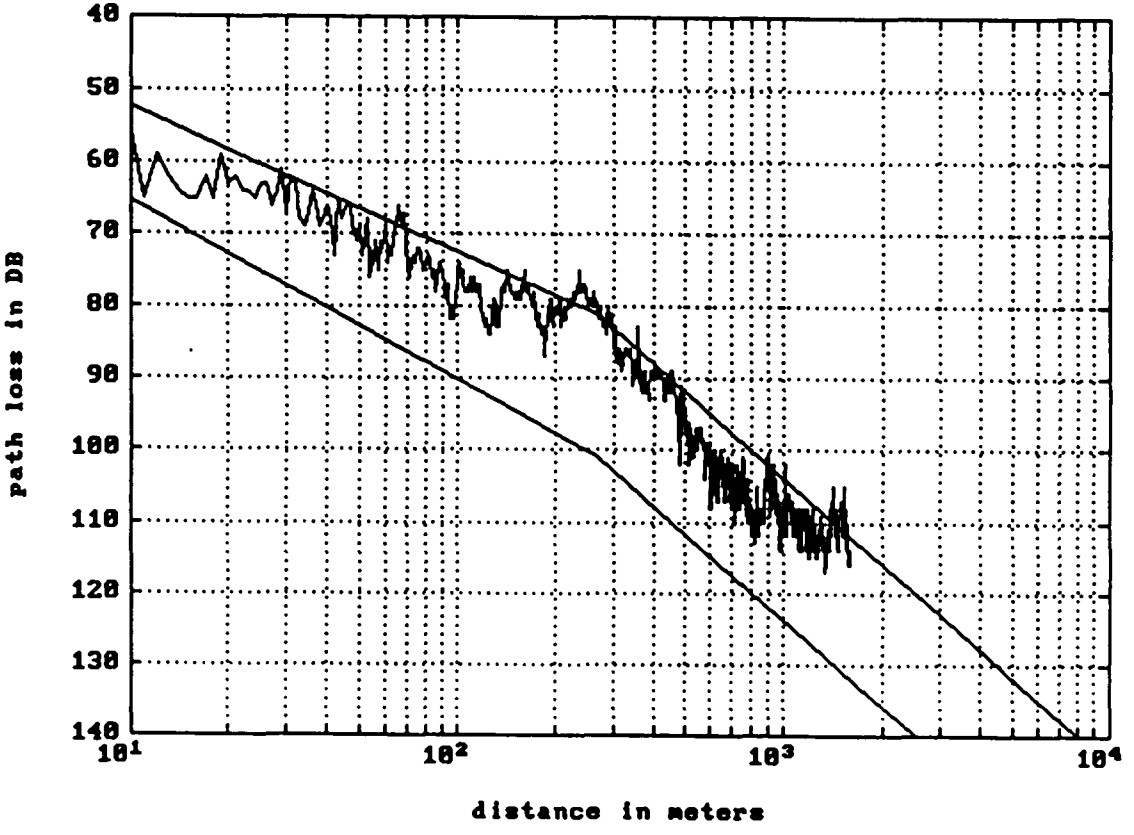

Figure 5.3.7 Urban area experimental data h_b=6.1m , h_m=1.5m

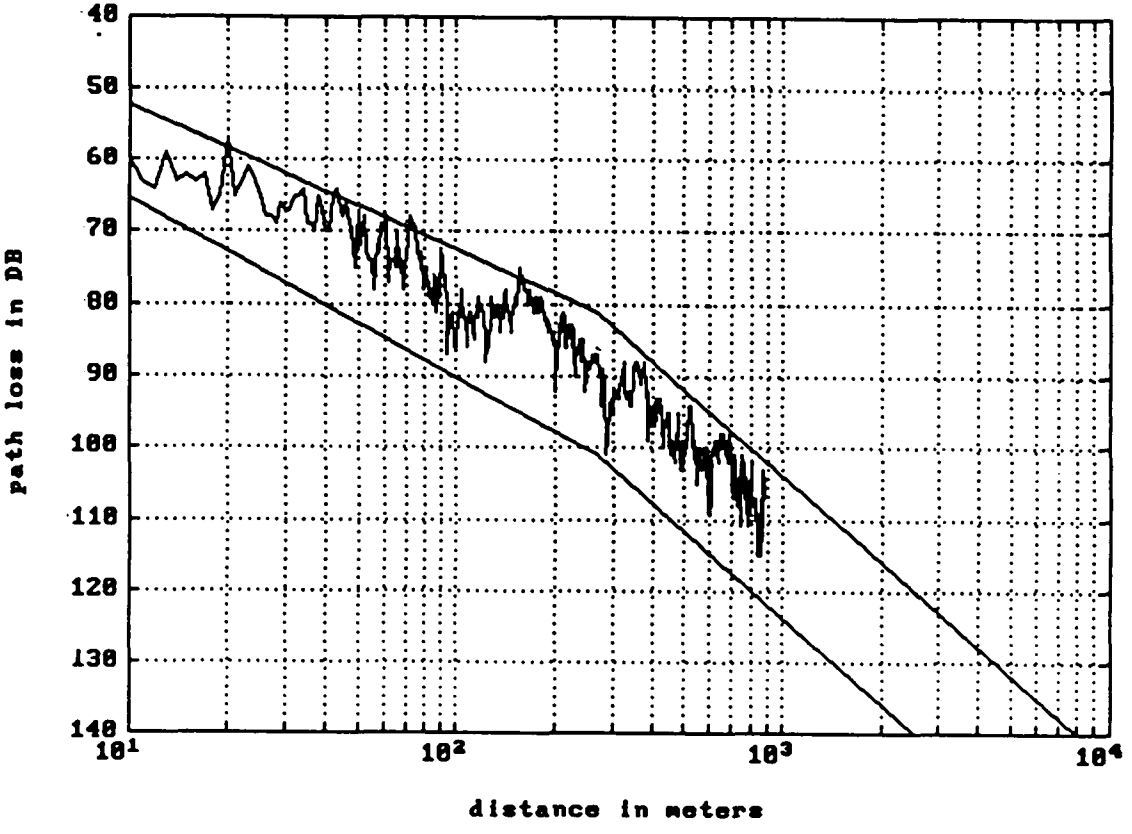

Figure 5.3.8 Urban area experimental data h_b=6.1m , h_m=1.5m

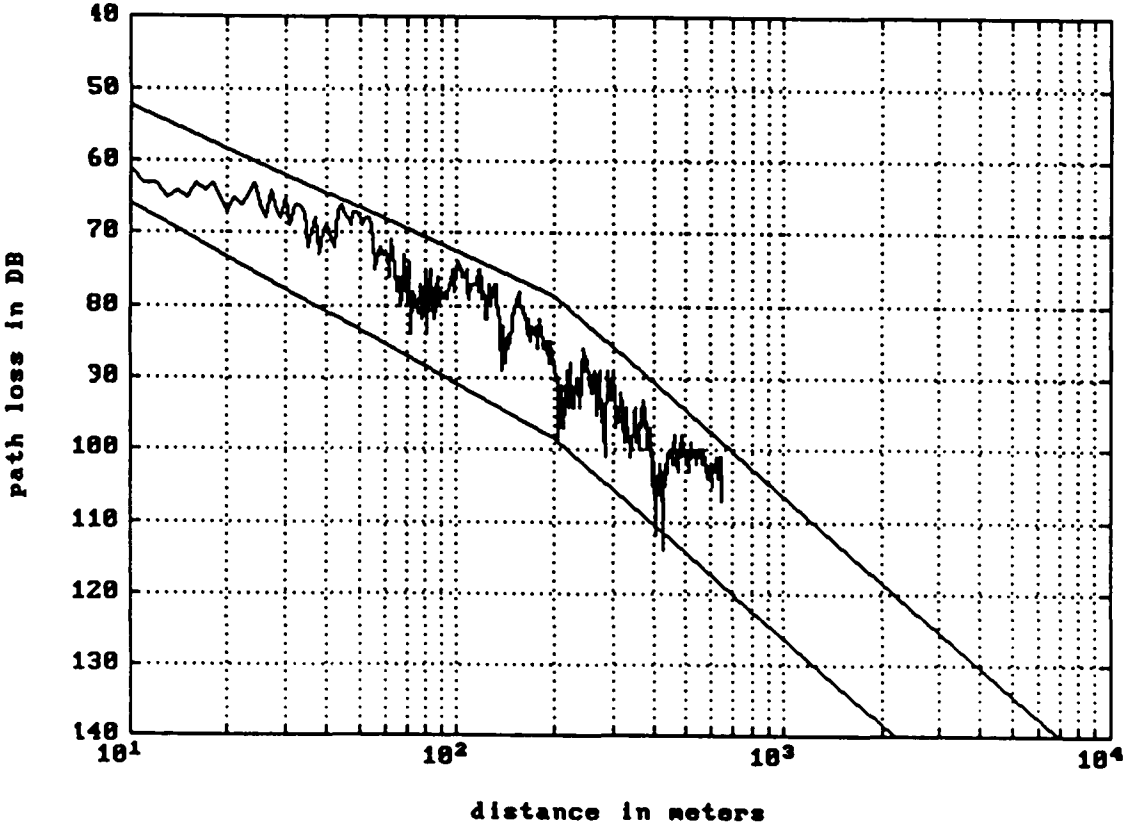

Figure 5.3.9 Suburban area experimental data h_b=5m , h_m=1.5m

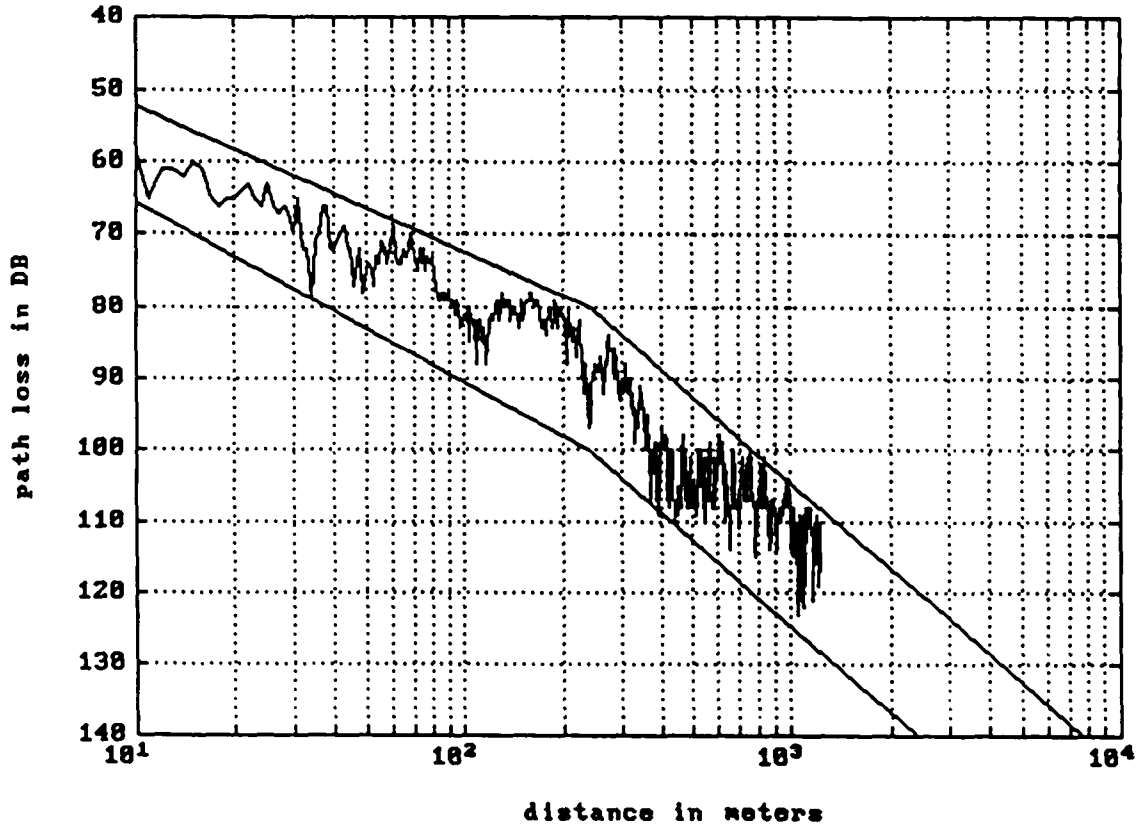

Figure 5.3.10 Suburban area experimental data h_b=6.1m , h_m=1.5m

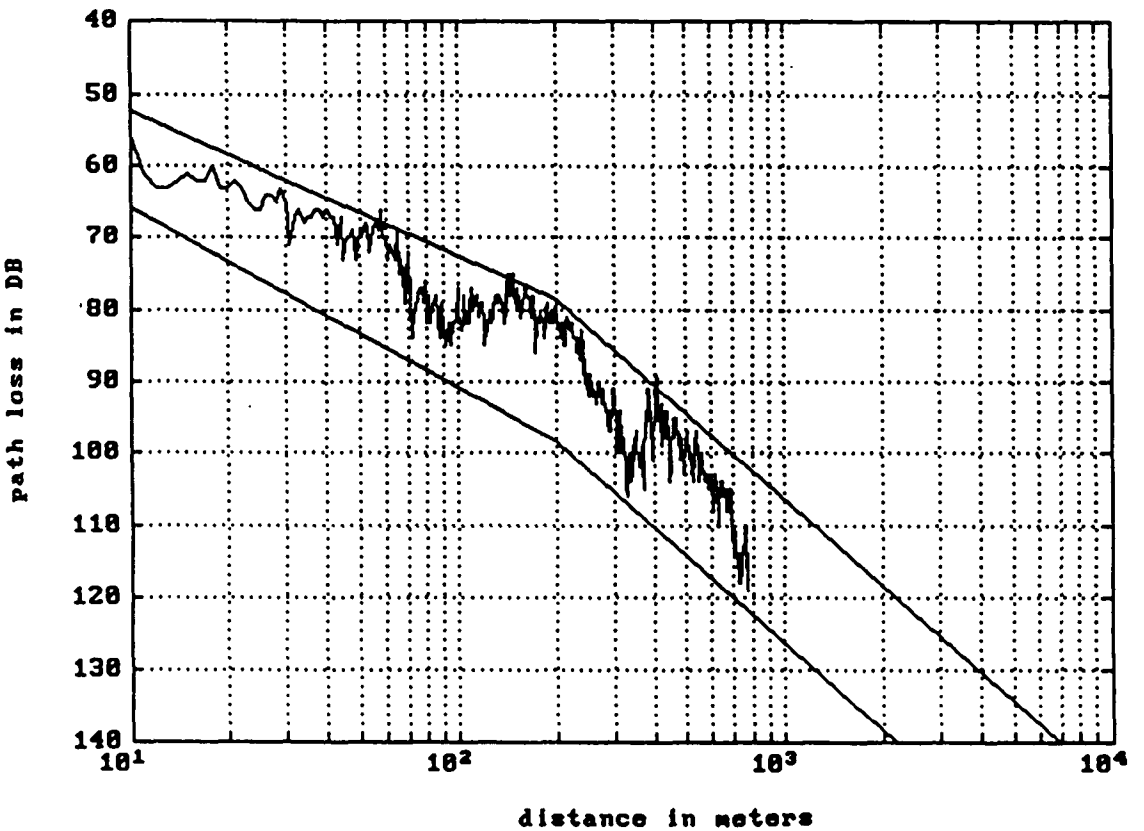

Figure 5.3.11 Suburban area experimental data h_b=5m , h_m=1.5m

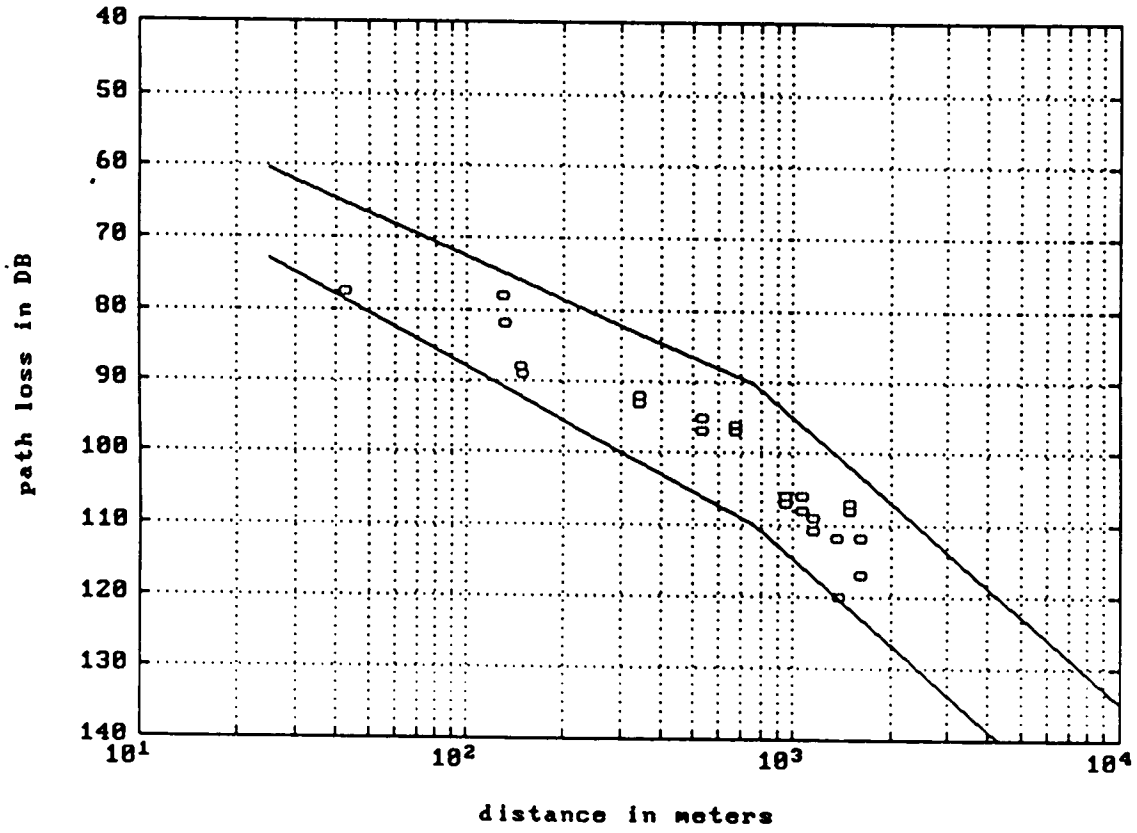

Figure 5.3.12 Urban area experimental data h_b=13.1m , h_m=2.2m

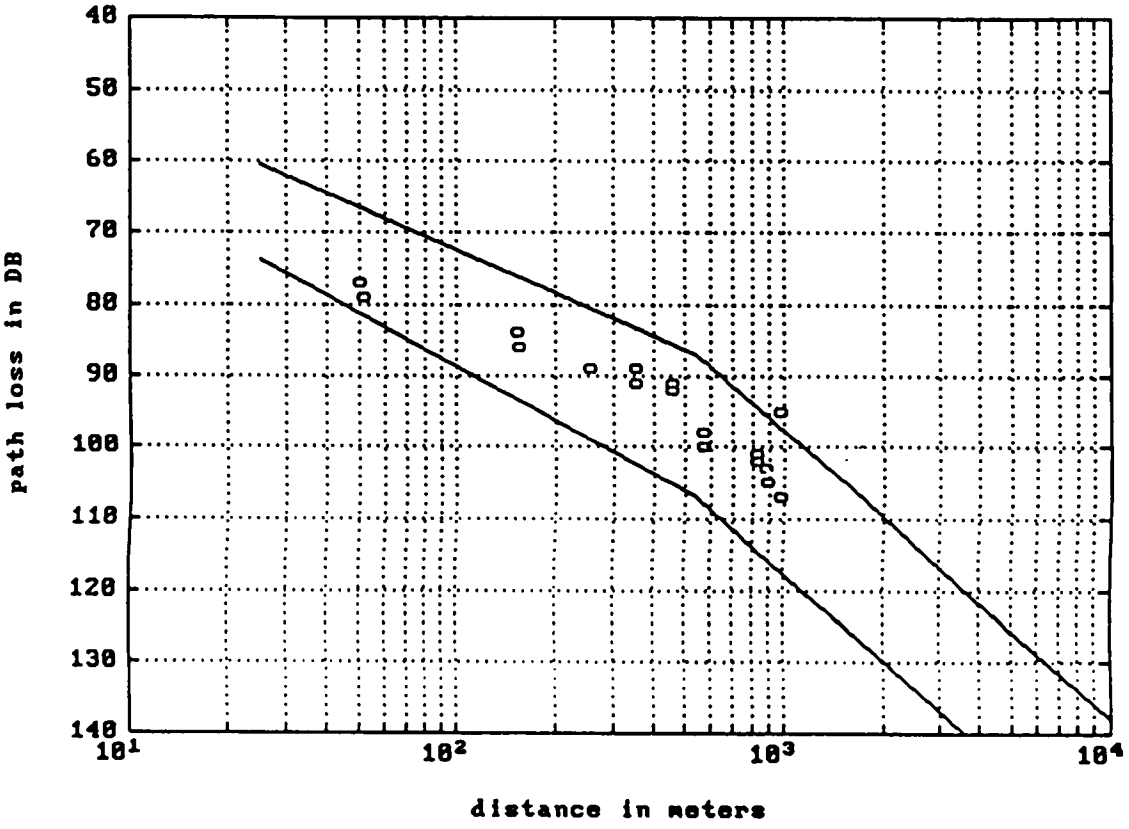

Figure 5.3.13 Urban area experimental data h_b=9.1m , h_m=2.2m

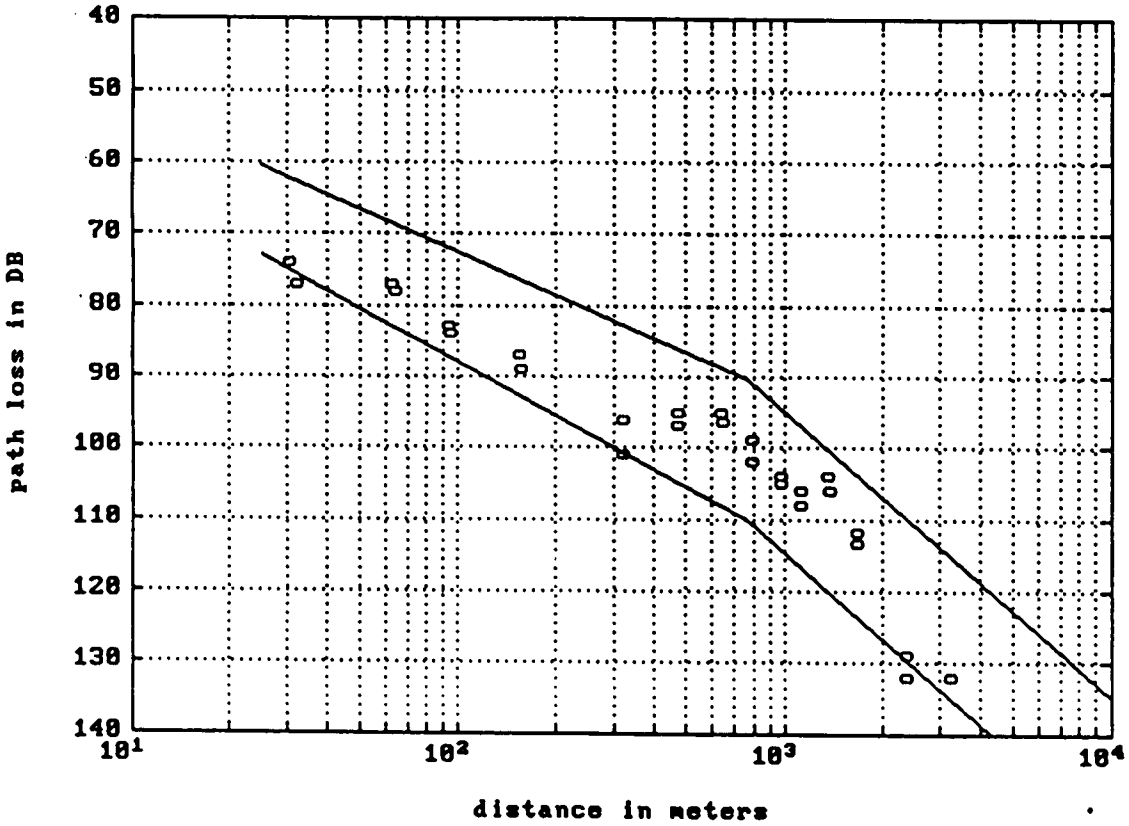

Figure 5.3.14 Suburban area experimental data h_b=13.1m , h_m=2.2m

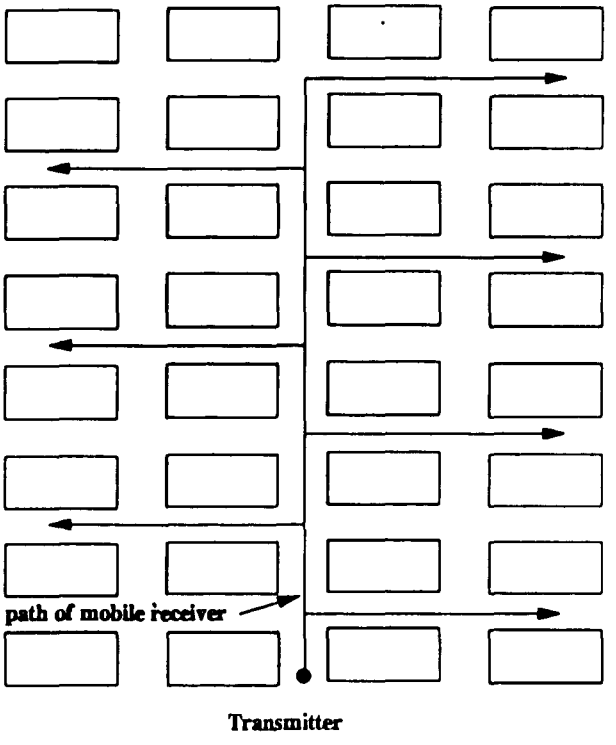

Figure 6.1.1 Out-of-sight propagation

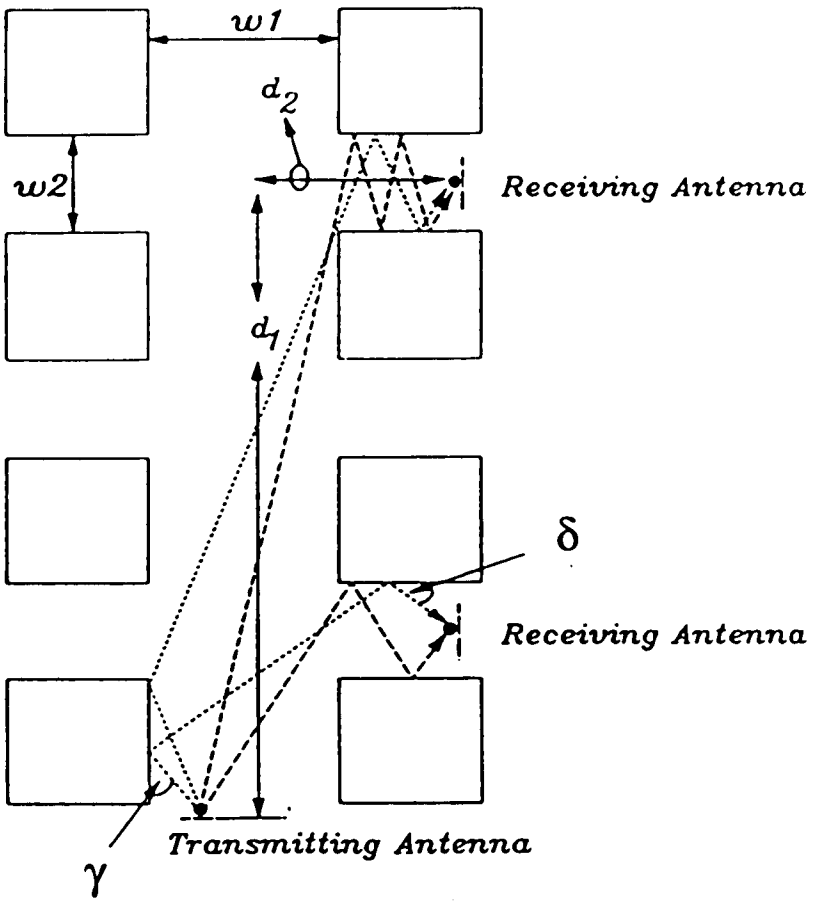

Figure 6.2.1 Rays entering out-of-sights streets

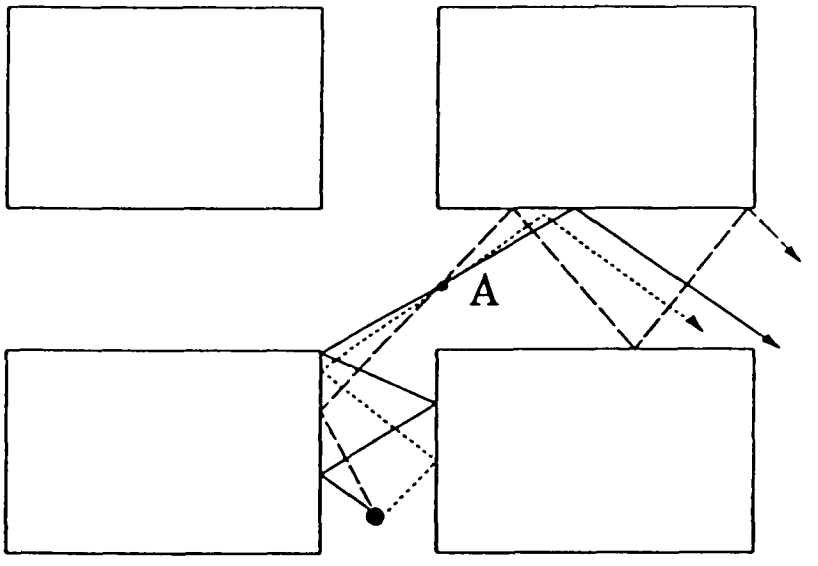

Figure 6.2.2

Only the rays passing through Point A are summed

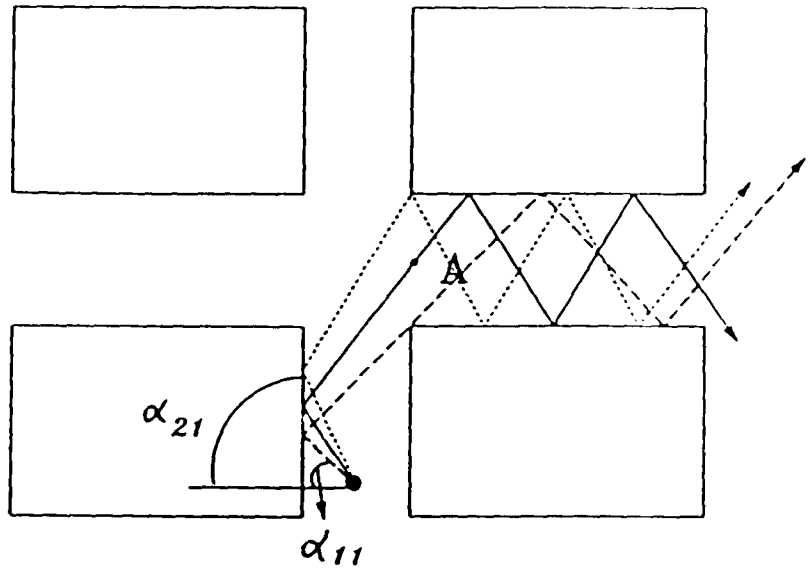

Figure 6.2.3

Rays with the minimum angle α_{11} and the maximum angle α_{21} of rays which leave the transmitter and which enter the out-of-sight street

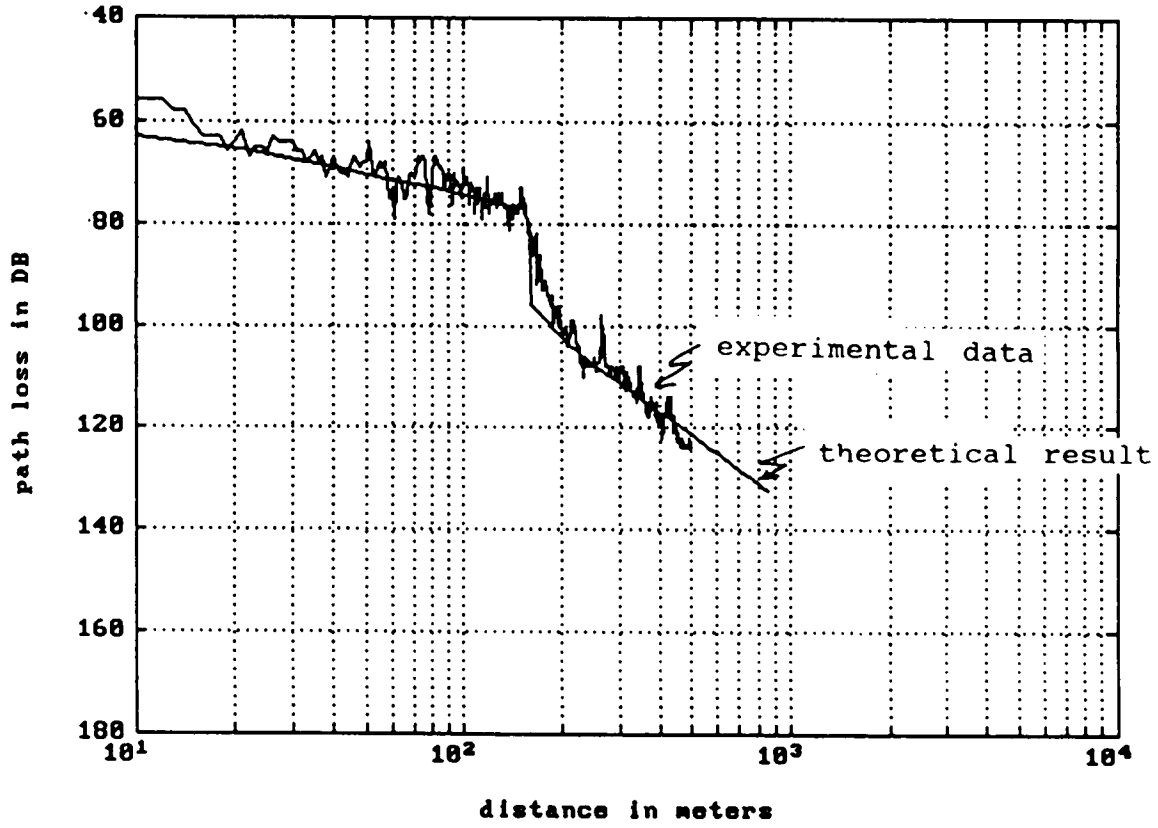

Figure 6.2.4 Manhattan, out-of-sight propagation (d_1 = 160m, h_b = 6.6m)

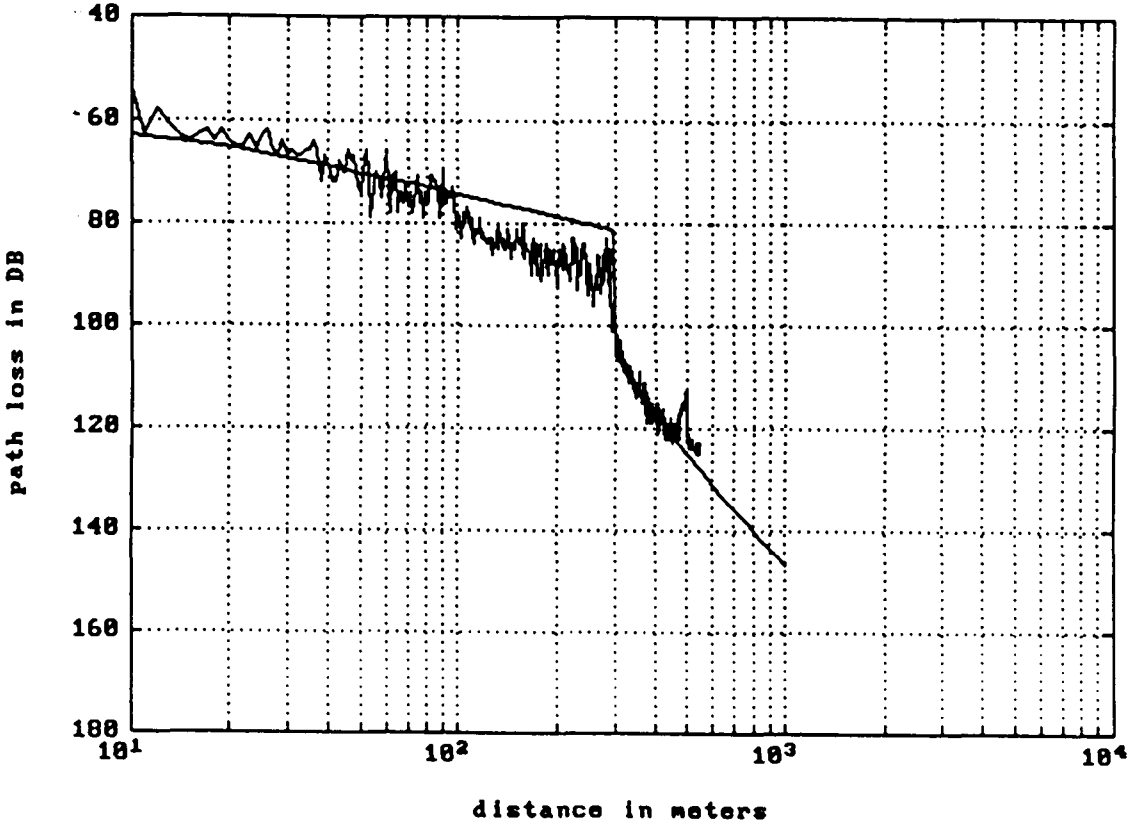

Figure 6.2.5 Manhattan, out-of-sight propagation (d_1 =290m, h_b = 6.6m)

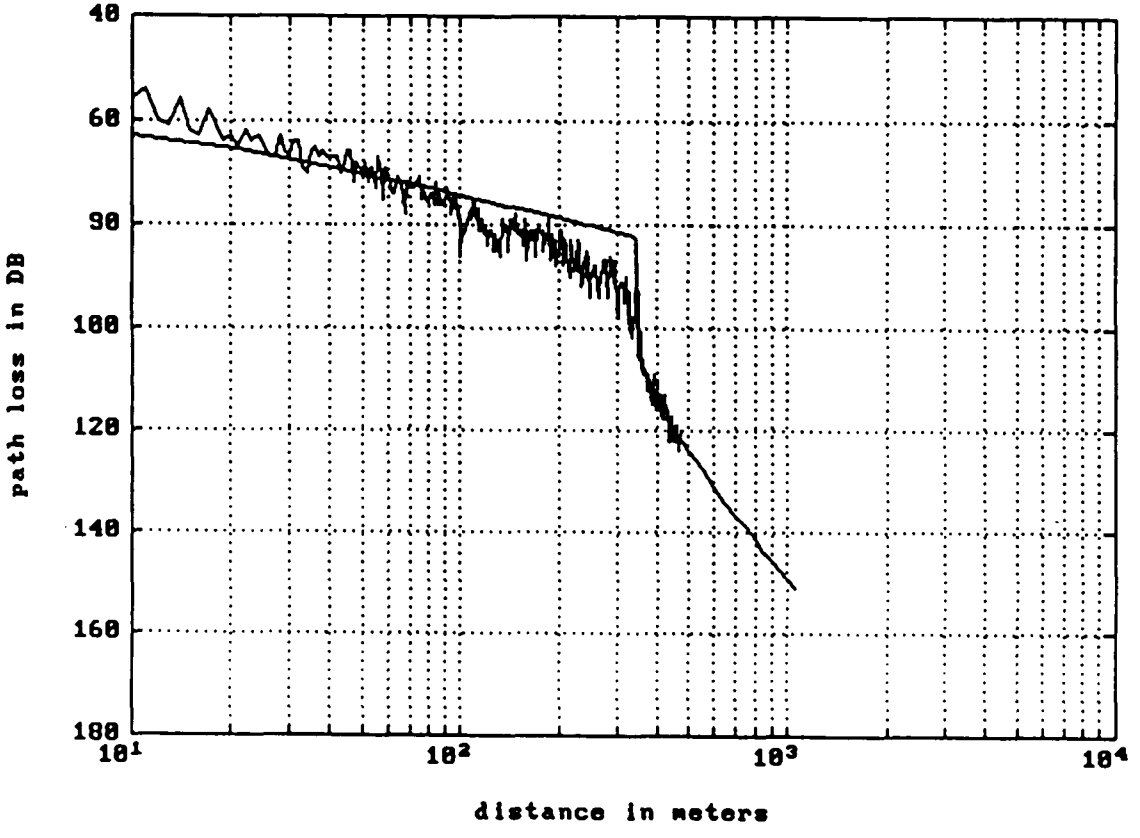

Figure 6.2.6 Manhattan, out-of-sight propagation (d_1 = 360m, h_b = 6.6m)

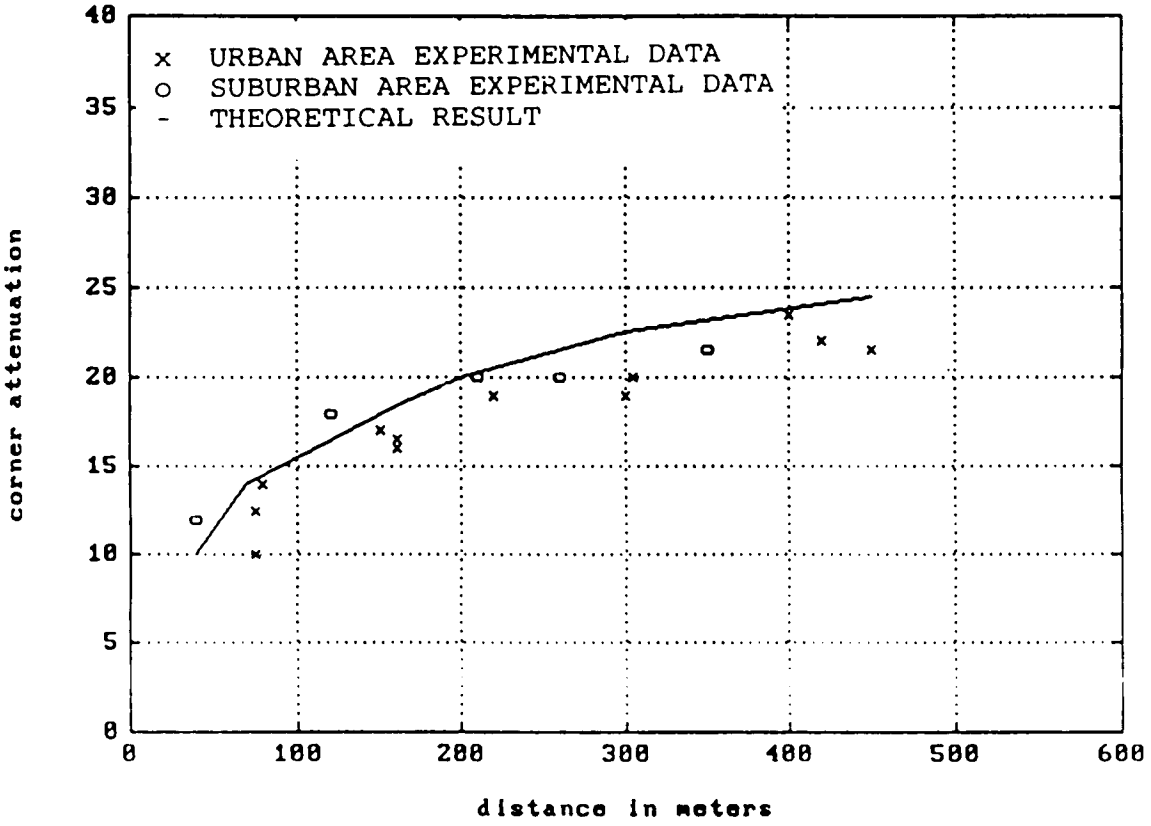

Figure 6.2.7 All of the urban and suburban experimental data plotted together with the theoretical result for the turning corner attenuation.

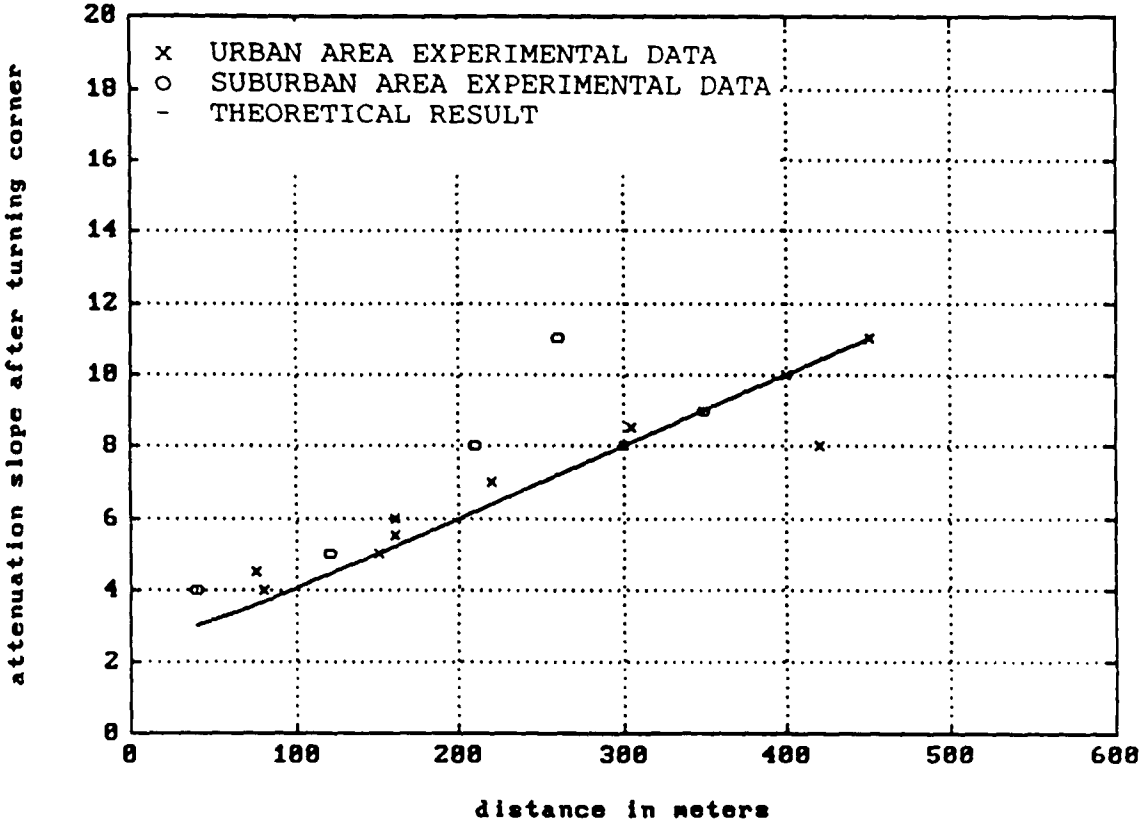

Figure 6.2.8 All of the urban and suburban experimental data plotted together with the theoretical result for the attenuation vs. distance slope.

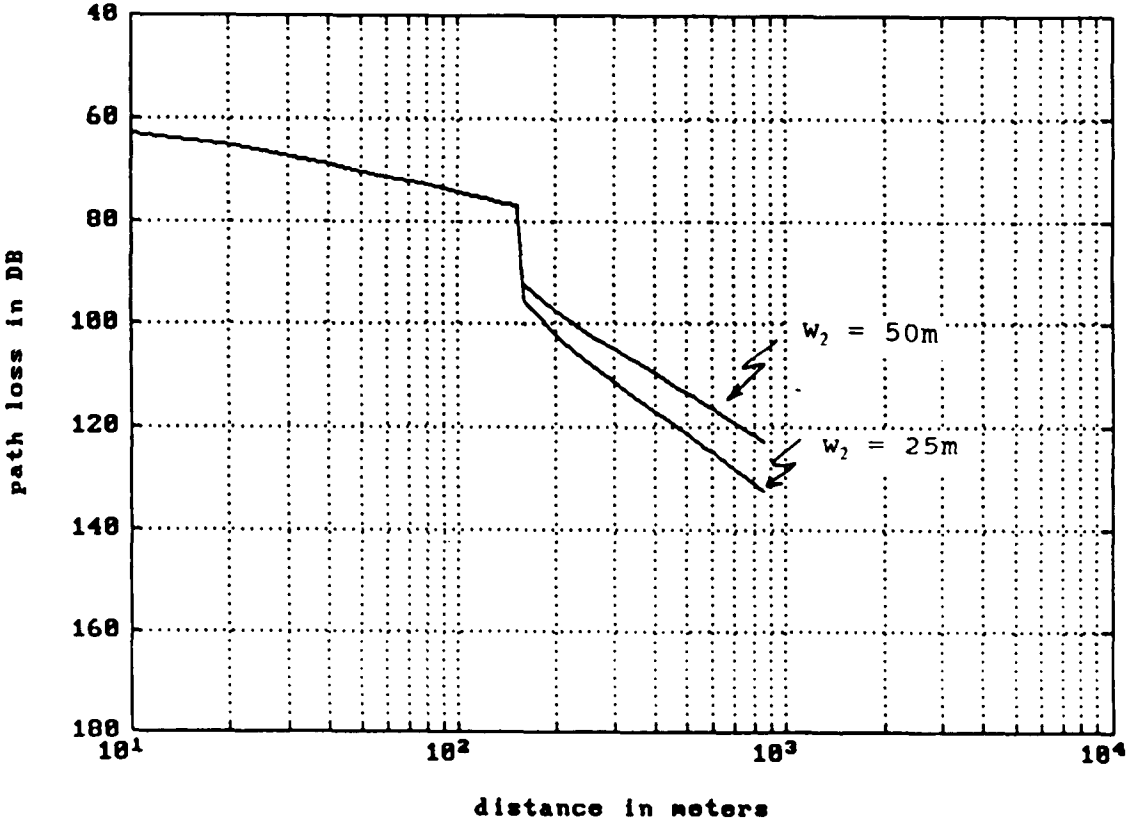

Figure 6.2.9 Out-of-sight propagation (computer evaluation) for d_1 = 160m, w_2 = 25m and w_2 = 50m.

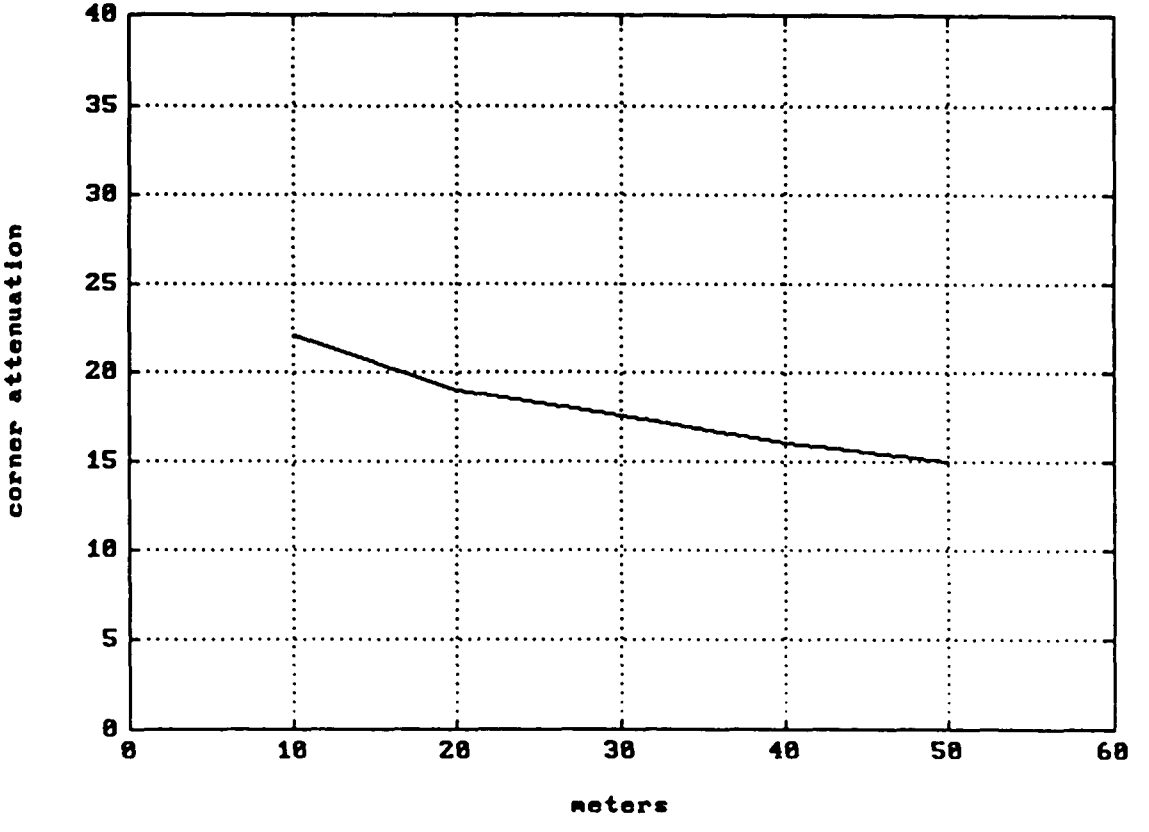

Figure 6.2.10 Out-of-sight propagation (computer evaluation for the corner attenuation) d_1 = 160m , w_2=10-50m

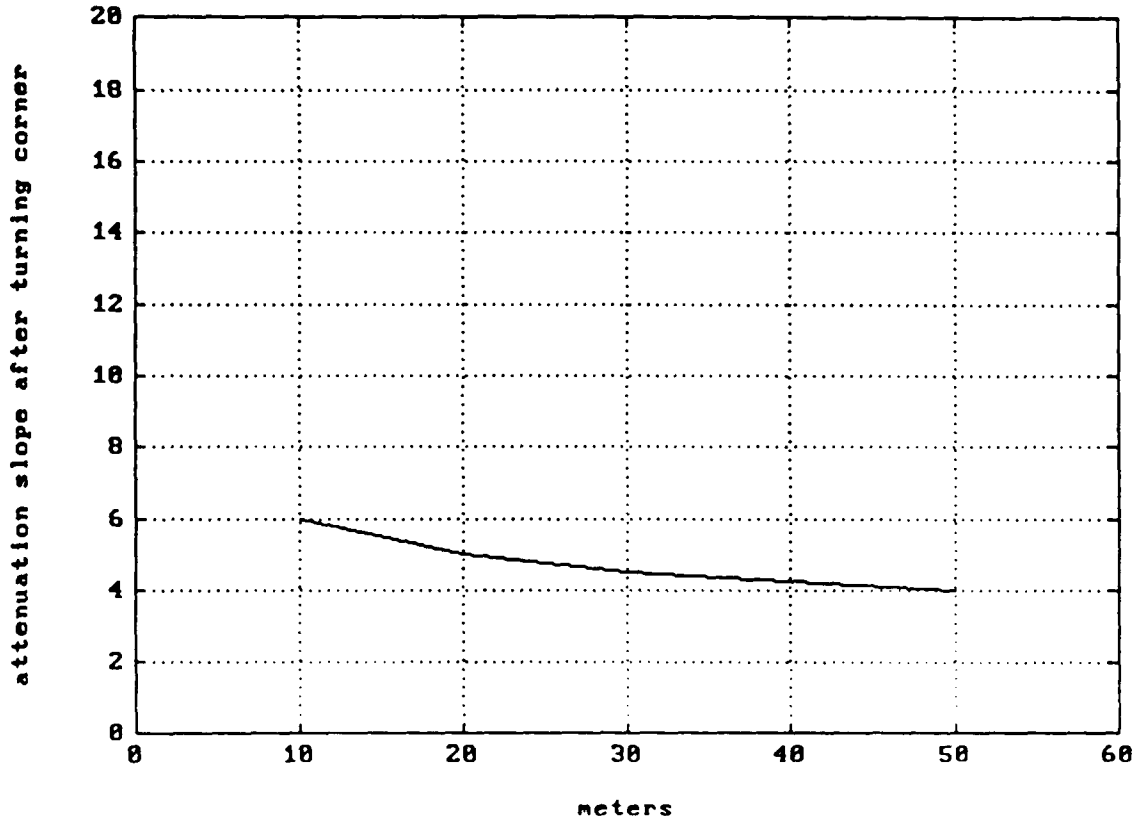

Figure 6.2.11 Out-of-sight propagation (computer evaluation for the slope) d_1 = 160m , w_2=10-50m

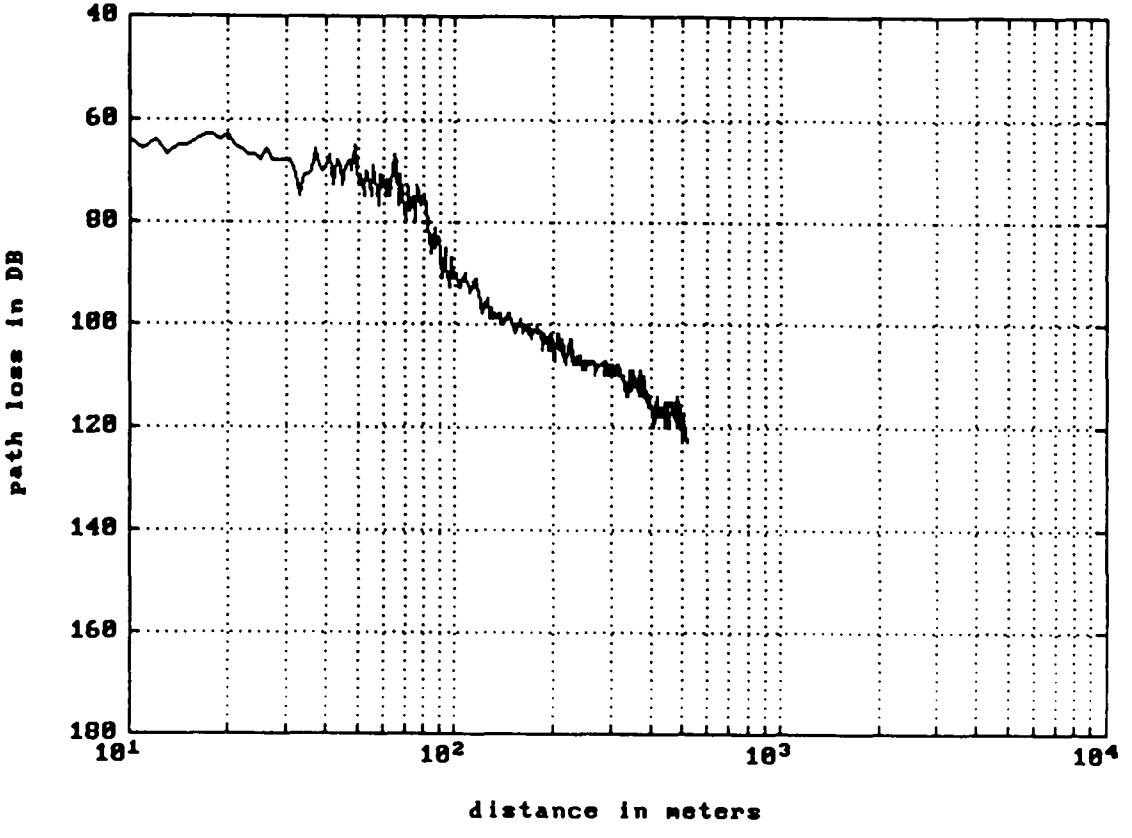

Figure 6.2.12 Manhattan, out-of-sight propagation (d_1 = 70m, h_b = 6.6m)

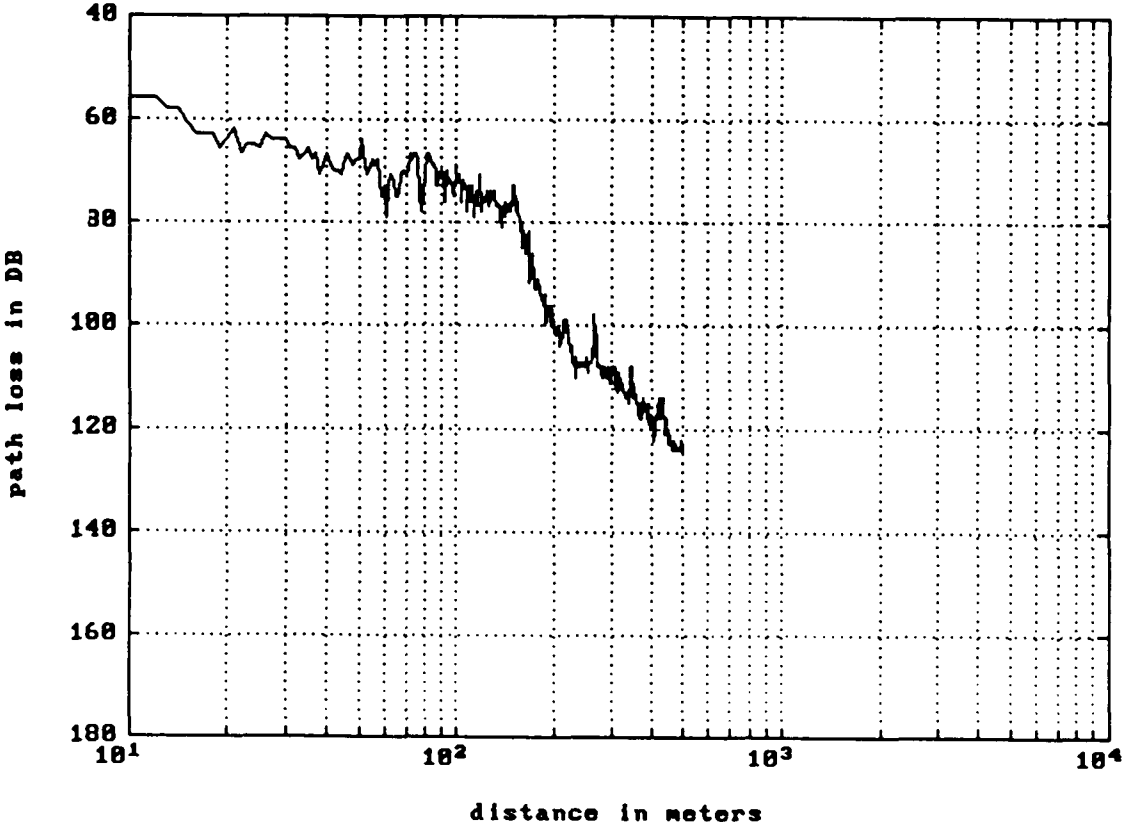

Figure 6.2.13 Manhattan, out-of-sight propagation (d_1 = 160m, h_b= 6.6m)

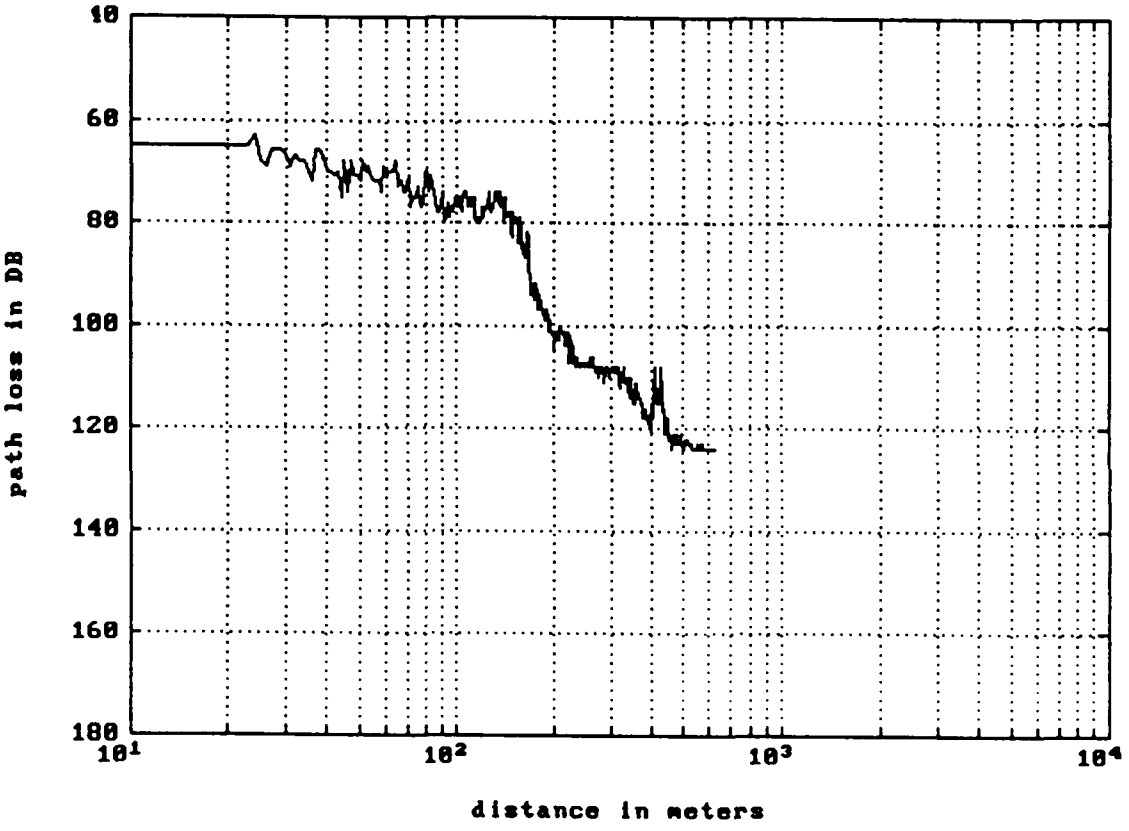

Figure 6.2.14 Manhattan, out-of-sight propagation (d_1 = 160m, h_b= 6.6m)

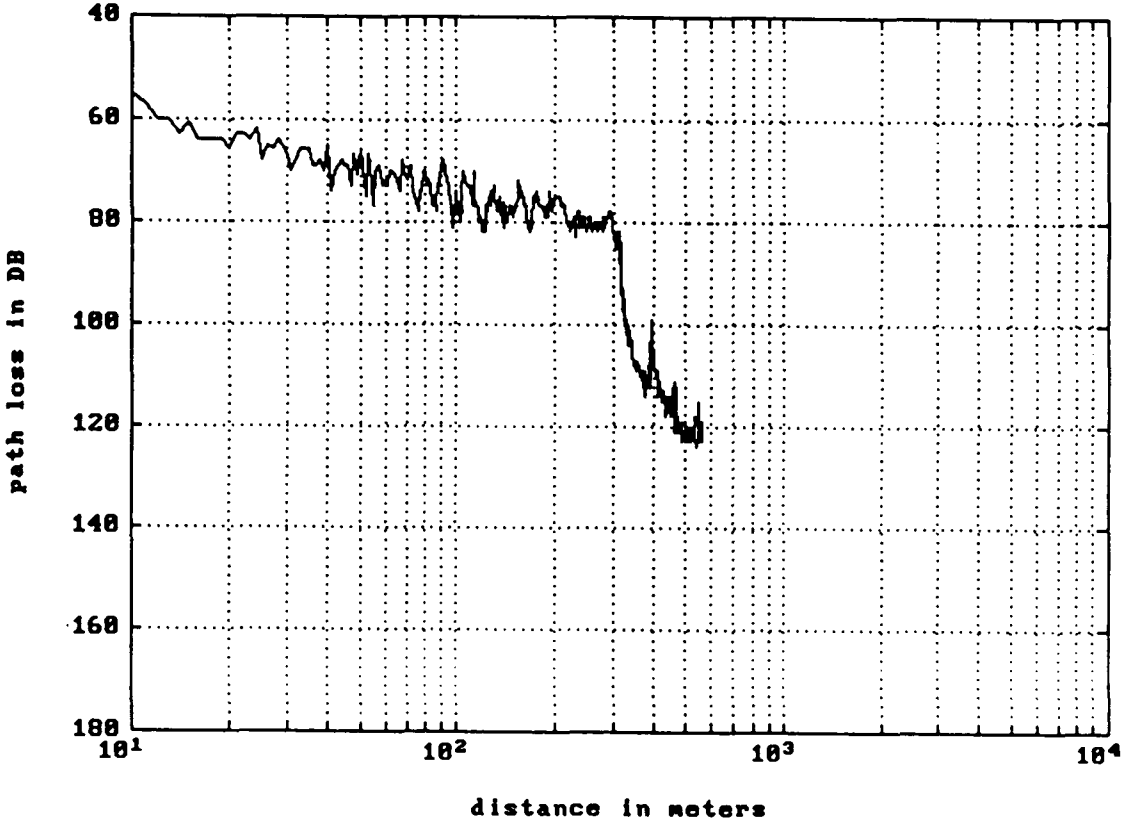

Figure 6.2.15 Manhattan, out-of-sight propagation (d_1 = 300m, h_b= 6.6m)

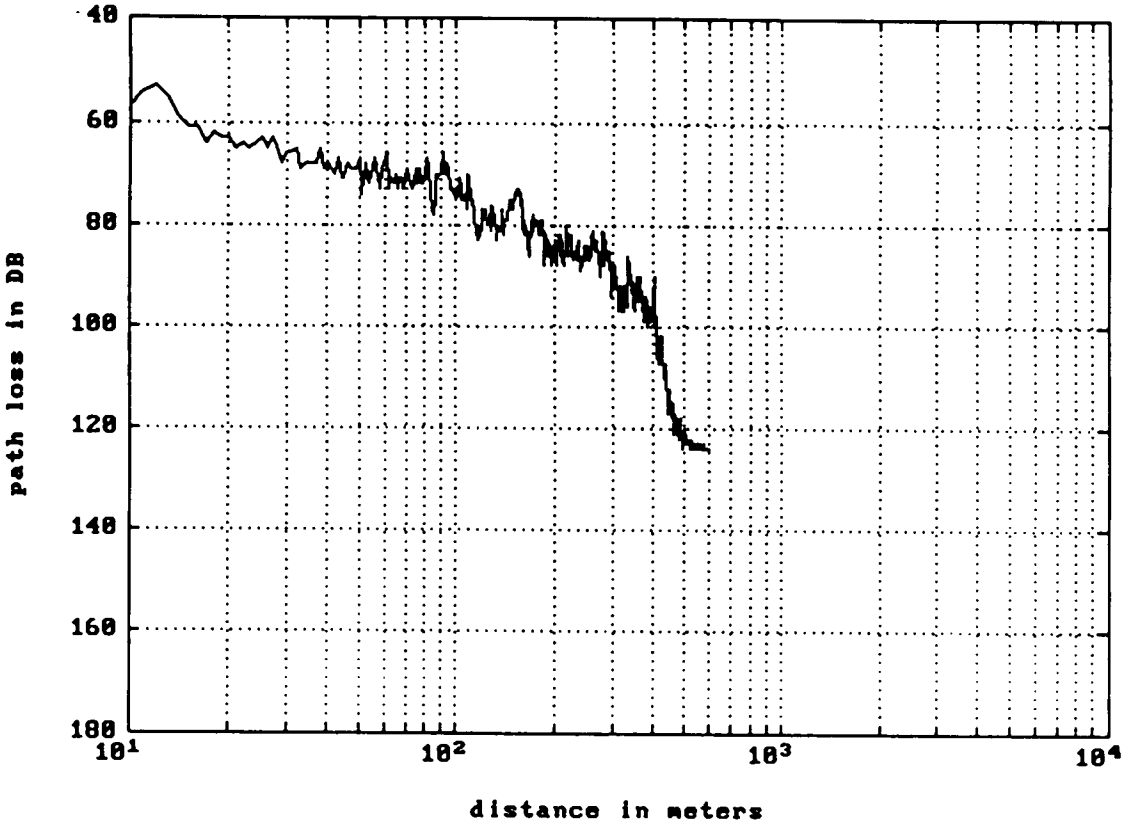

Figure 6.2.16 Manhattan, out-of-sight propagation (d_1 = 410m, h_b= 6.6m)

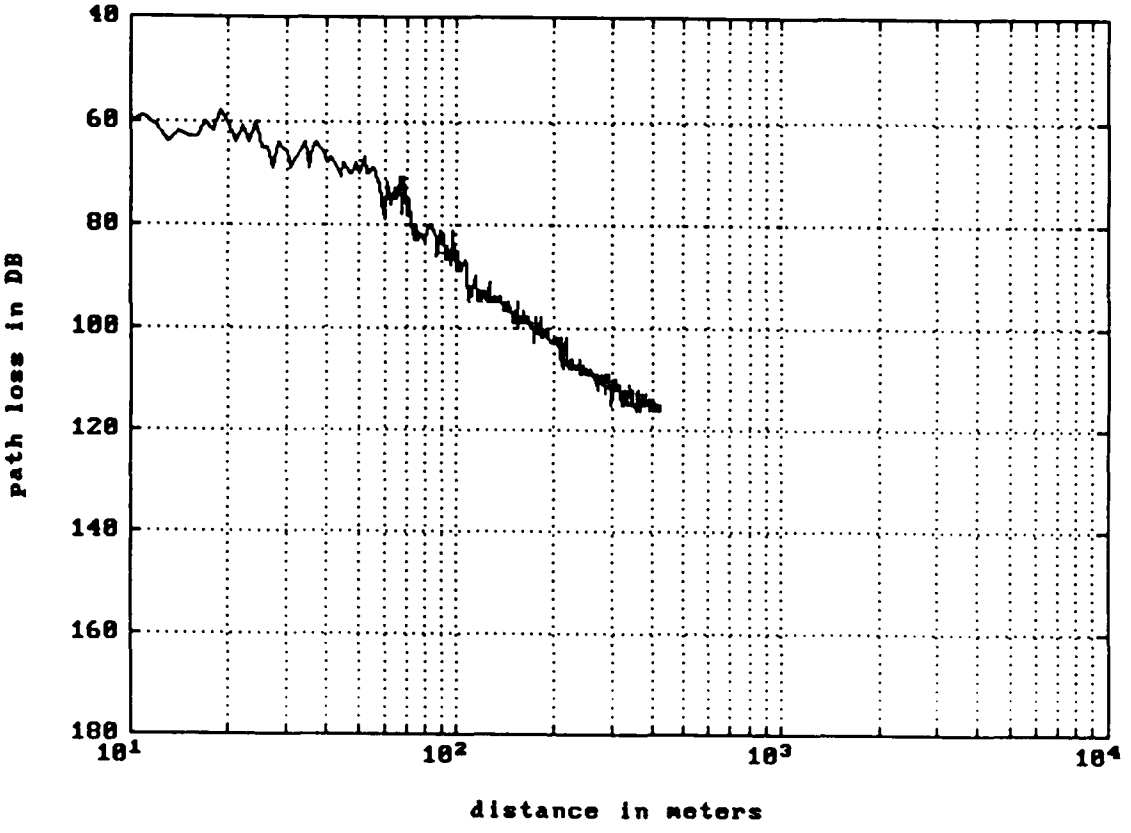

Figure 6.2.17 Manhattan, out-of-sight propagation (d_1 = 70m, h_b = 3.3m)

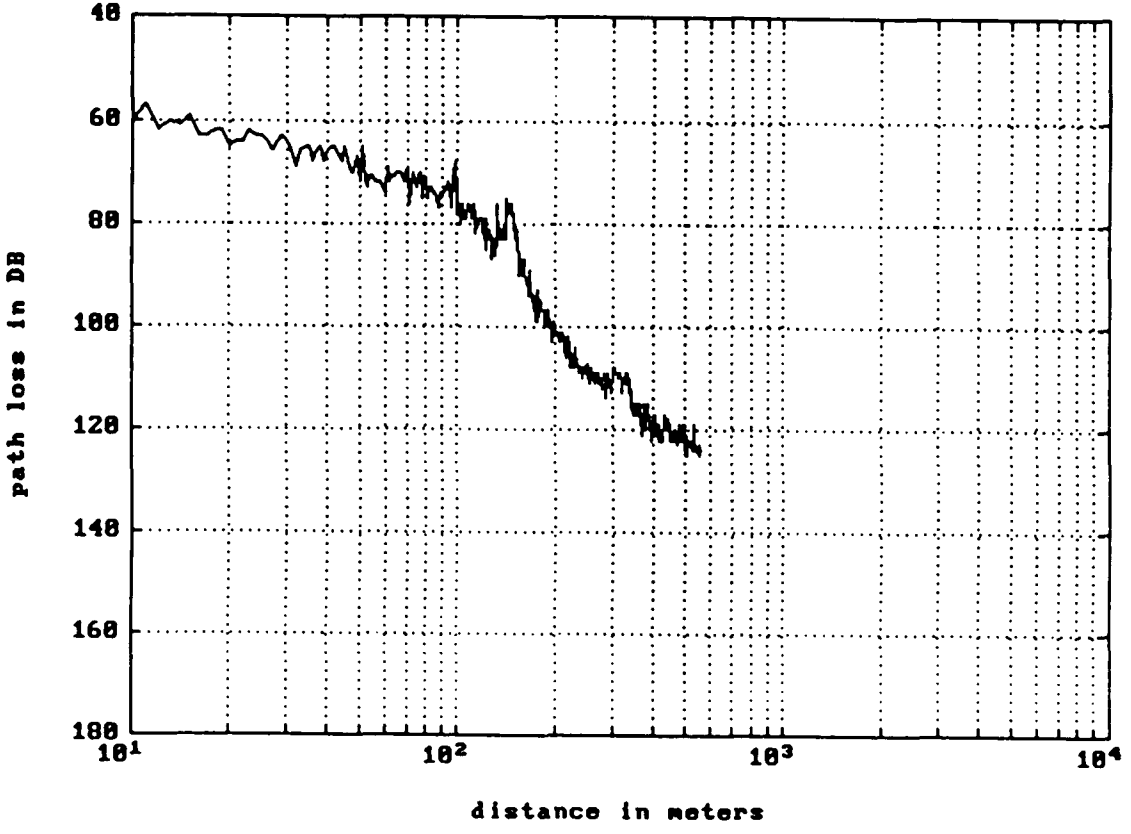

Figure 6.2.18 Manhattan, out-of-sight propagation (d_1 = 160m, h_b= 3.3m)

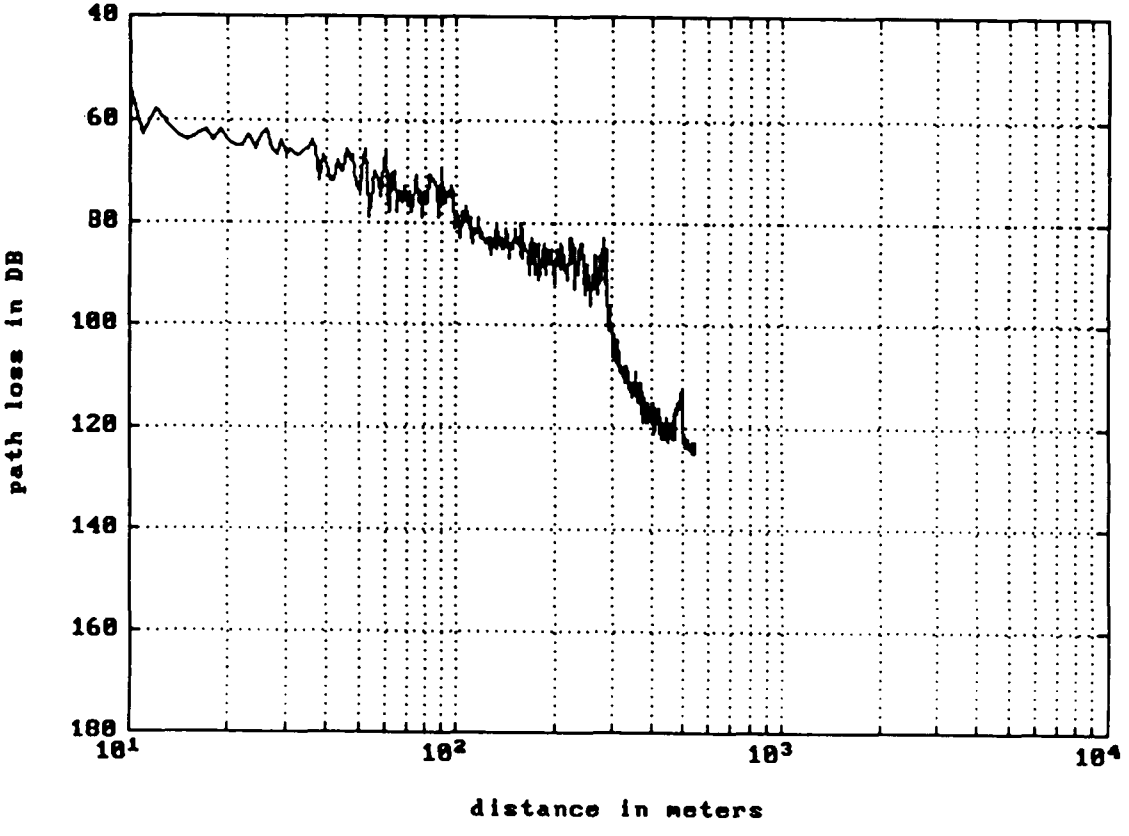

Figure 6.2.19 Manhattan, out-of-sight propagation (d_1 = 290m, h_b= 3.3m)

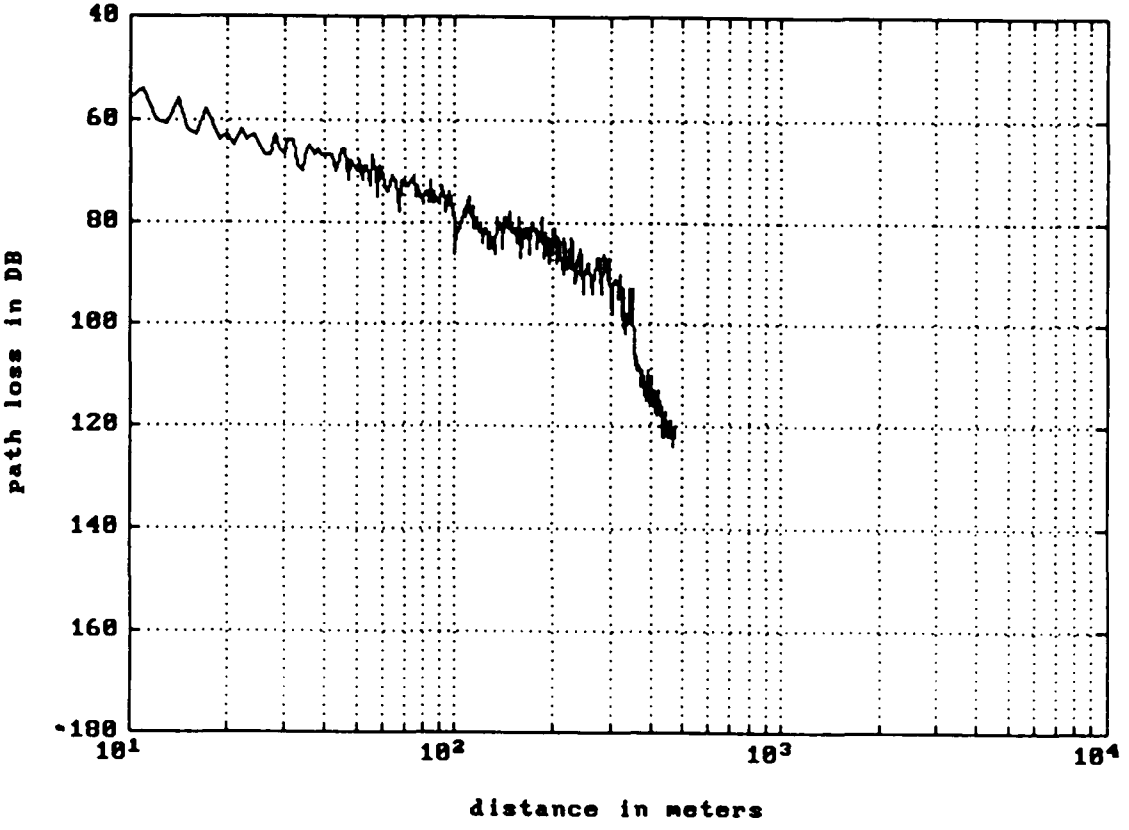

Figure 6.2.20 Manhattan, out-of-sight propagation (d_1 = 360m, h_b= 3.3m)

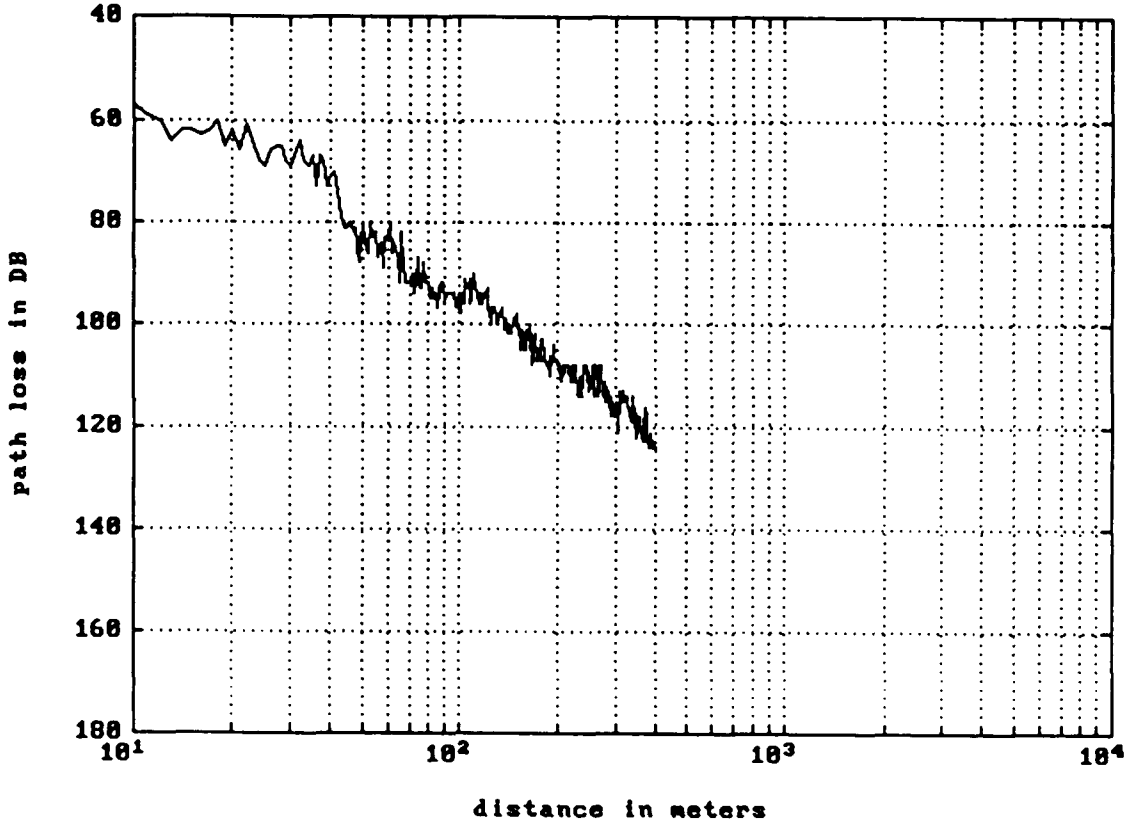

Figure 6.2.21 Flushing, out-of-sight propagation (d_1 = 40m, h_b = 6.6m)

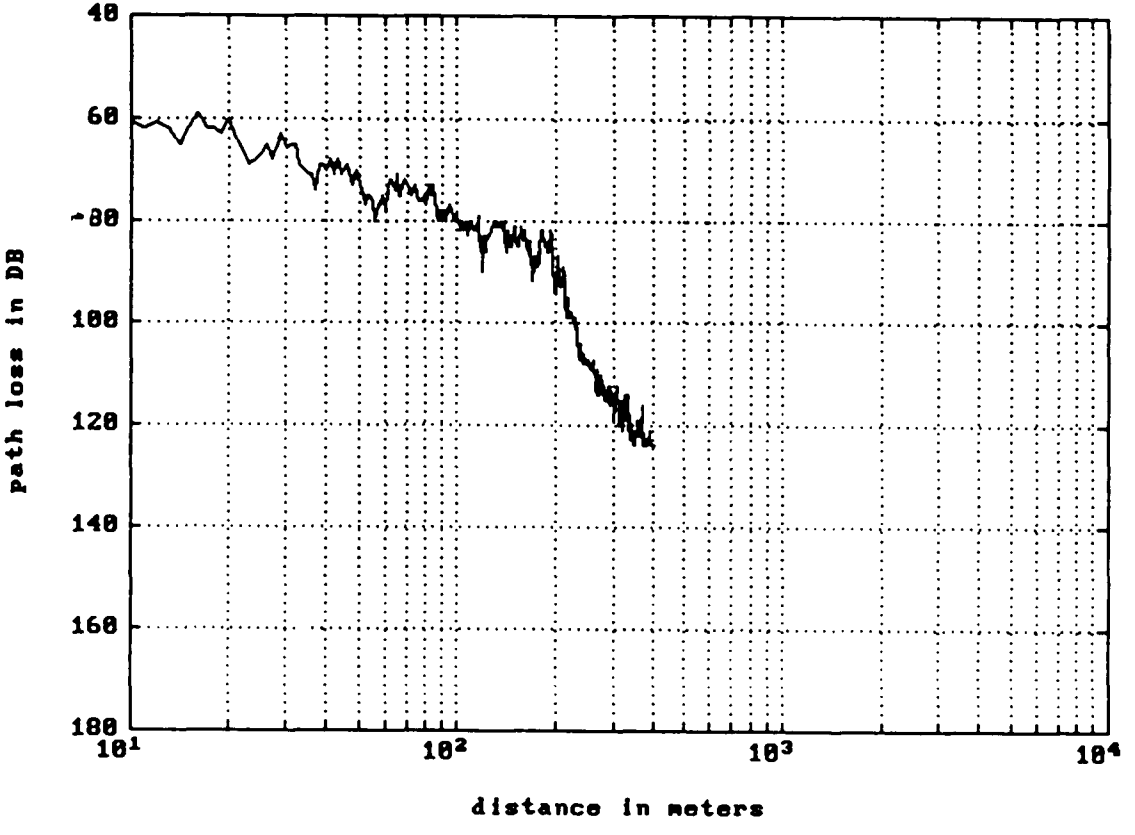

Figure 6.2.22 Flushing, out-of-sight propagation (d_1 = 210m, h_b = 6.6m)

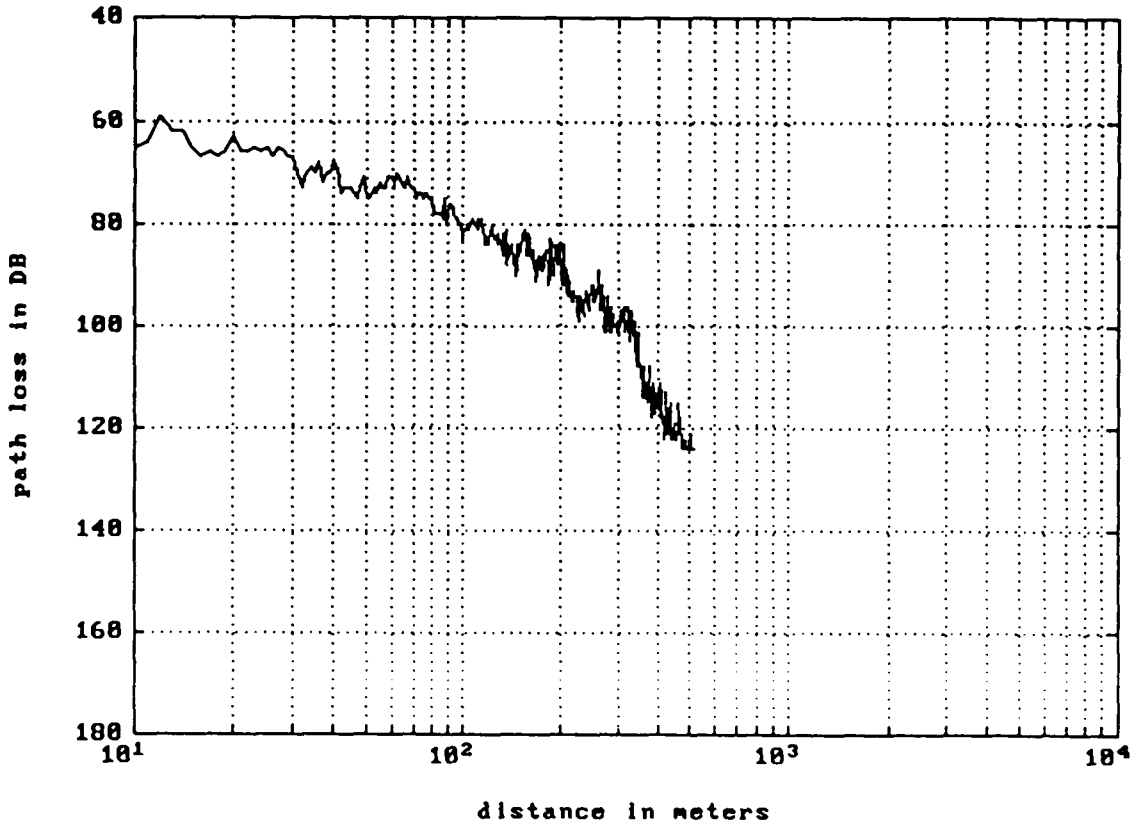

Figure 6.2.23 Flushing, out-of-sight propagation (d_1 = 330m, h_b = 6.6m)

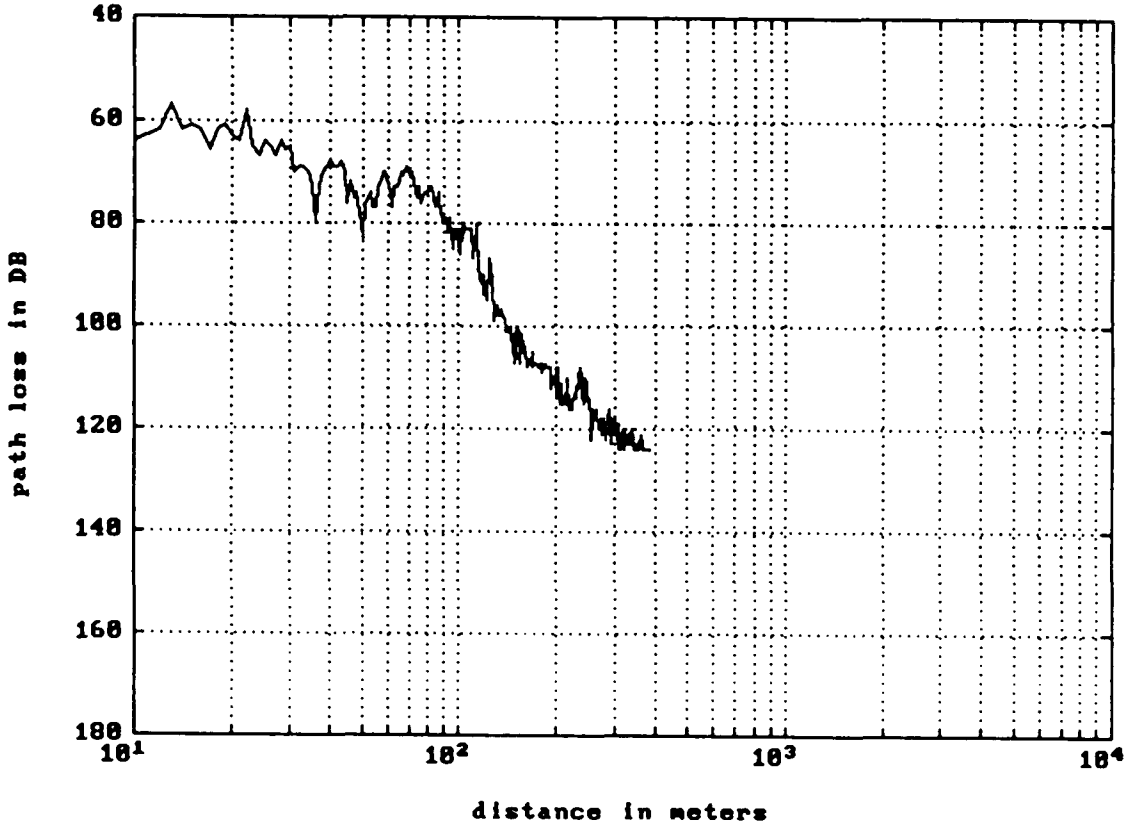

Figure 6.2.24 Flushing, out-of-sight propagation (d_1 = 120m, h_b = 6.6m)

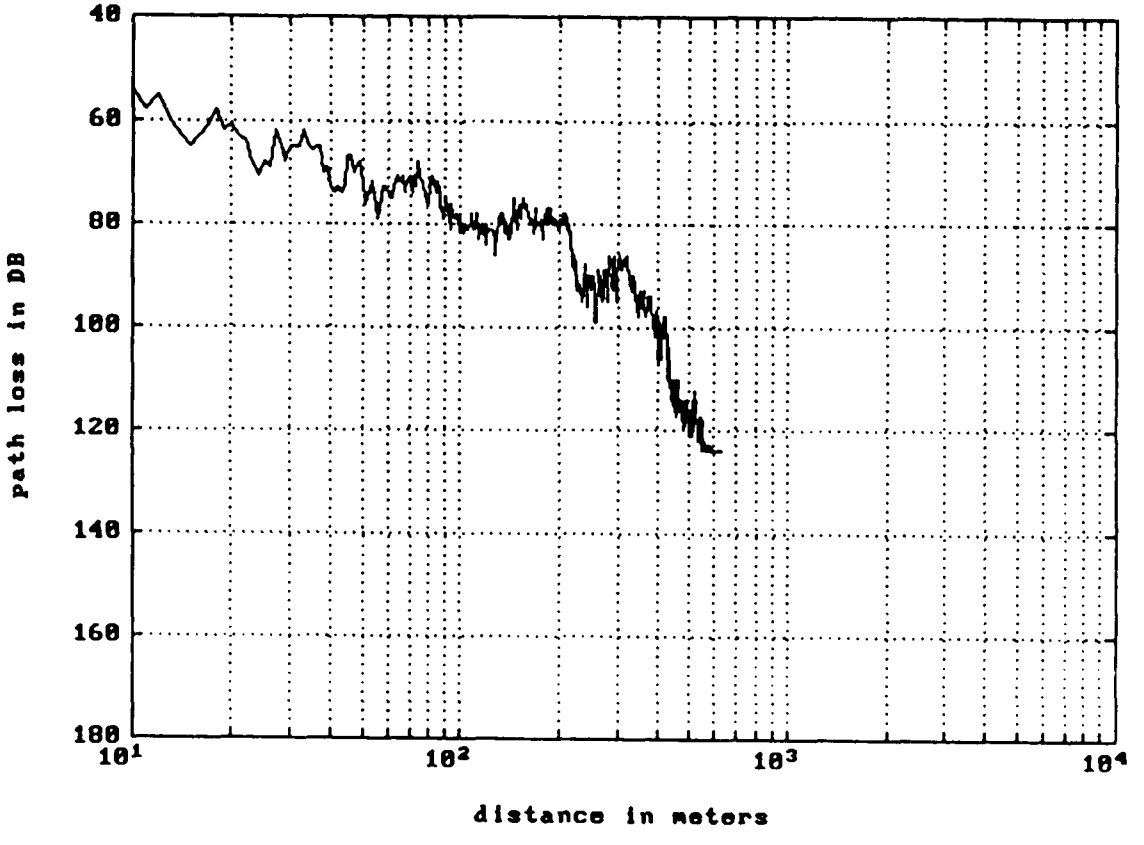

Figure 6.2.25 Flushing, out-of-sight propagation (d_1 = 420m, h_b = 6.6m)

9 REFERENCES

[1] W.C.Y. Lee, "Smaller cells for greater performance," IEEE Communications Magazine, pp. 19-23, November 1991.

[2] R. Steele and V.K. Prabhu, "Higher user density digital cellular mobile radio systems," Proc. Inst. Elec. Eng., part. F, vol. 132, no. 5, pp. 396-404, August 1985.

[3] R. Steele, "The cellular environment of lightweight handheld portables," IEEE Communications Magazine, vol. 27, no. 7, pp.20-29, July 1989.

[4] D.C. Cox, "Portable digital radio communications - An approach to tetherless access," IEEE Communications Magazine, vol. 7, no. 7, pp. 30-40, July 1989.

[5] H. Taub and D.L. Schilling, "Principles of communication systems," New York: McGraw-Hill, 1986.

[6] D.L. Schilling, L.B. Milstein, R.L. Pickholtz, F. Bruno, E. Kanterakis, V. Erceg, M. Kullback, W.H. Biederman, D. Fishman, and D. Salerno, "Field test experiments using Broadband Code Division Multiple Access," IEEE Communications Magazine, pp. 86-93, November 1991.

[7] L.B. Milstein, D.L. Schilling, R.L. Picholtz, V. Erceg, M. Kullback, E. Kanterakis, D. Fishman, W.H. Biederman,

and D. Salerno, "On the feasibility of a CDMA overlay for personal communication networks," IEEE Journal on Selected Areas in Communications, pp. 655-668, May 1992.

[8] R.L. Picholtz, L.B. Milstein, and D.L. Schilling, "Spread spectrum for mobile communications," IEEE Transactions on Vehicular Technology, pp. 313-322, May 1991.

[9] R.G. Vaughan, "Signals in mobile communications: a review," IEEE Transactions on Vehicular Technology, vol. VT-35, no. 4, pp. 133-144, November 1986.

[10] D.O. Reudnik, "Properties of mobile radio propagation above 400 MHz," IEEE Transactions on Vehicular Technology, vol. VT-23, no. 4, pp. 143-159, November 1974.

[11] J. M. Holtzman and L.M.A. Jalloul, "Rayleigh fading effect reduction with wideband DS/CDMA signals," Globecom Conference, Phoenix, AR, December 1991.

[12] P.F. Sass, "Propagation measurements for UHF spread spectrum mobile communications," IEEE Transactions on Vehicular Technology, vol. VT-32, no. 2, pp. 168-176, May 1983.

[13] G.Y. Delisle, J.P. Lefevre, M. Lecours, and J.Y. Chouinard, "Propagation loss prediction: a comparative

study with application to mobile radio channel," IEEE Transactions on Vehicular Technology, vol. VT-34, no. 2, pp. 86-96, May 1985.

[14] B.R. Davis and R.E. Bogner, "Propagation at 500 MHz for mobile radio," Proc. Inst. Eng., part F, no. 5, pp. 307 - 320, August 1985.

[15] J.W. Whitteker, "Measurements of path los at 910 MHz for proposed microcell urban mobile systems," IEEE Transactions on Vehicular Technology, vol. 37, no. 3 pp. 125-129, August 1988.

[16] S.Y. Seidel, T.S. Rappaport, S. Jain, M.L. Lord, and R. Singh, "Path loss, scattering, and multipath delay statistics in four european cities for digital cellular and microcellular radiotelephone," IEEE Transactions on Vehicular Technology, vol. 40, no. 4, pp. 721-730, November 1991.

[17] M. Hata, K. Kinoshita, and K. Hirade, "Radio link design of cellular land mobile communication systems," IEEE Transactions on Vehicular Technology, vol. VT-31, no. 1, pp. 25-31, February 1982.

[18] A.J. Rustako, N. Amitay, G.J. Owens, and R.S. Roman, "Radio propagation measurements at microwave frequencies for microcellular mobile and personal communications,"

in Proc. ICC, Boston, MA, pp. 482-486, June 1991.

[19] A.J. Rustako, N. Amitay, G.J. Owens, and R.S. Roman, "Propagation measurements at microwave frequencies for microcellular mobile and personal communications," in Proc. 39th IEEE Vehicular Technology Conference, San Francisco, CA, pp. 316-320, May 1989.

[20] W.C.Y. Lee, "Studies of base-station antenna height effects on mobile radio," IEEE Transactions on Vehicular Technology, vol. VT-29, no. 2, pp. 252-260, May 1980.

[21] D. C. Cox, "910 MHz urban mobile radio propagation multipath characteristics in NYC," IEEE Transactions on Vehicular Technology, vol. VT-22, no. 4, pp. 104-110, November 1973.

[22] T.S. Rappaport and L.B. Milstein, "Effects of path loss and fringe user distribution on CDMA cellular frequency reuse efficiency," Globecom Conference, San Diego, CA, pp. 500-505, December 1990.

[23] M. Hata, "Empirical formula for propagation loss in land mobile radio services," IEEE Transactions on Vehicular Technology, vol. VT-29, no. 3, pp. 317-325, August 1980.

[24] A.J. Rustako, N. Amitay, G.J. Owens, and R.S. Roman, "Radio propagation at microwave frequencies for line-of

sight microcellular mobile and personal communications," IEEE Transactions on Vehicular Technology, vol.40, no. 1, pp. 203-210, February 1991.

[25] E. Green and M. Hata, "Microcellular propagation measurements in an urban environment," IEEE International Symposium on Personal, Indoor and Mobile Radio Communication, London, GB, pp. 324-328, September 1991.

[26] P. Harley, "Short distance attenuation measurements at 900 MHz and 1.88 GHz using four antenna heights for microcells," IEEE Journal on Selected Areas in Communications, vol.7, no. 1, pp. 5-11, January 1989.

[27] K. Bullington, "Radio propagation for vehicular technology", IEEE Transactions on Vehicular Technology, vol.VT-26, no. 4, pp. 295-308, November 1977.

[28] W.C.Y. Lee, "Mobile communications engineering," New York: McGraw Hill, pp. 93, 1982.

[29] Y. Nagata, Y. Furuya, E. Moriyama, M. Mizuno, I. Kamiya, and S. Hattori, "Measurement and modeling of 2 GHz-band out-of-sight radio propagation characteristics under microcellular environments," IEEE International Symposium on Personal, Indoor and Mobile Radio Communication, London, GB, pp. 341-346, September 1991.

[30] L.L. Nagy, "Electromagnetic reflectivity characteristics of road surfaces," IEEE Transactions on Vehicular Technology, vol. VT-23, no. 4, pp. 117-124, November 1974.